SMITHSONIAN CONTRIBUTIONS TO THE EARTH SCIENCES • NUMBER 13

Distinctive Properties of Turbiditic and Hemipelagic Mud Layers in the Algéro-Balearic Basin, Western Mediterranean Sea

Nicolaas A. Rupke
and Daniel Jean Stanley

SMITHSONIAN INSTITUTION PRESS
City of Washington
1974

ABSTRACT

Rupke, Nicolaas A., and Daniel Jean Stanley. Distinctive Properties of Turbiditic and Hemipelagic Mud Layers in the Algéro-Balearic Basin, Western Mediterranean Sea. *Smithsonian Contributions to the Earth Sciences,* number 13, 40 pages, 21 figures, 8 tables, 1974.—Two types of mud layers alternate in dominantly muddy cores of the southern Balearic Basin. Type A muds (a few cm to over 50 cm thick), macroscopically homogeneous, occur above turbidite sands or silt laminae. Type B muds (imperceptible to about 50 cm thick), comparatively coarse due to interspersed microskeletons, occur below turbidite sands or silt laminae, and lie above type A muds. The two types are distinguished in X-radiographs on the basis of texture and sedimentary structures. Type A and B mud layers in six cores were sampled at 1 to 8 cm intervals.

Type A muds are distribution graded (upward shift of the entire size distribution to finer sizes), continuing the upward grading of the underlying sand turbidites. A granulometric change occurs at the boundary with type B muds which contain sand (to 16 percent), largely tests of forams and pteropod shells. The sand fraction of type A muds ($\leqslant$ 1 percent) differs from that of type B in the proportion of terrigenous constituents and in remains of pelagic forams and of pteropods. Type B muds are not graded; their grain-size distribution is uniform. They have a higher (26 to 46 percent) carbonate content than type A (16 to 39 percent). In some instances, peak-height ratios of clay minerals change across the boundary between type A and type B mud layers. It is concluded that type A muds are turbiditic (deposited instantaneously), while B muds are hemipelagic deposits.

Carbon-14 ages were determined on the carbonate sand fraction of type B layers. The ages were plotted against the total sediment thickness above the dated samples in each core. A statistically significant correlation exists. However, when the turbiditic sand and mud layers are omitted and the ages are plotted only against the combined thicknesses of the hemipelagic type B layers, an even stronger correlation is obtained. The hemipelagic rate of sedimentation during the past 16,000 years approximates 10 cm/1000 years. The frequency of turbidity current incursions at a particular core location averages 3 per 2000 years.

OFFICIAL PUBLICATION DATE is handstamped in a limited number of initial copies and is recorded in the Institution's annual report, *Smithsonian Year.* SI PRESS NUMBER 5089. SERIES COVER DESIGN: Aerial view of Ulawun Volcano, New Britain.

Library of Congress Cataloging in Publication Data
Rupke, Nicolaas A.
Distinctive properties of turbiditic and hemipelagic mud layers in the Algéro-Balearic Basin, western Mediterranean Sea.
(Smithsonian contributions to the earth sciences, no. 13)
Supt. of Docs. no.: SI 1.26: 13.
1. Marine sediments—Western Mediterranean. 2. Turbidites—Western Mediterranean. I. Stanley, Daniel Jean, joint author. II. Title. III. Series: Smithsonian Institution. Smithsonian contributions to the earth science, no. 13.
QE1.S227 no. 13. [GC389] 550'.8s [551.4'62'1] 74-1273

For sale by the Superintendent of Documents, U.S. Government Printing Office, Washington, D.C. 20402
Price 95 cents

Contents

Distinctive Properties of Turbiditic and Hemipelagic Mud Layers in the Algéro-Balearic Basin, Western Mediterranean Sea

Nicolaas A. Rupke
and Daniel Jean Stanley

Introduction

Graded sands and sandstones, alternating with fine-grained layers, form thick accumulations in modern deep-sea basins and in ancient geosynclinal belts, where they are called flysch. The deep-sea sands are generally believed to be the products of turbidity currents that transport coarse-grained sediments to the deep marine environment, smooth out topography, and construct abyssal plains (cf. summary by Horn, Ewing, and Ewing, 1972). A compelling amount of evidence points to a turbidity current emplacement of most flysch sandstones as well, in spite of some remaining problems (cf. review by Kuenen, 1967).

The flysch-type sands and sandstones exhibit a characteristic assemblage of internal and bedding plane structures. The internal sedimentary structures occur in a fixed succession of structural intervals or divisions, viz., a basal, graded division (*a*), a lower division of parallel lamination (*b*), a division of current ripple lamination (*c*), an upper division of parallel lamination (*d*), and a largely structureless, fine-grained or pelitic division (*e*) (Bouma, 1962, fig. 8). This succession of sedimentary structures, defined from ancient flysch sandstones, applies to modern deep-sea sands as well (cf. review by Walker, 1970). The interpretation of the flysch-type sands and sandstones as turbidity current deposits or turbidites is to a significant extent based on these sedimentary structures and their reproduction in experimental flume studies (summarized in Middleton, 1965).

In the fine-grained division (variously called pelite,[1] lutite, clay or shale layer, argillite, and mud[2] or mudstone layer), primary sedimentary structures are virtually absent. Accordingly, the question of the origin of the pelitic division is still largely unresolved and has often remained unaddressed in many publications on turbidite sequences. In most of the early, often classic, papers on tur-

Nicolaas A. Rupke and Daniel Jean Stanley: Division of Sedimentology, Department of Paleobiology, Smithsonian Institution, Washington, D.C. 20560. Rupke, present address: Department of Geology and Mineralogy, Oxford University, Oxford OX1 3PR, Great Britain.

[1] In this study we use the term "pelite," defined as a "sediment or sedimentary rock composed of the finest detritus (clay- or mud-size particles)" (AGI, *Glossary of Geology*, 1972).

[2] Mud is defined as "an unconsolidated sediment consisting of clay and/or silt, together with material of other dimensions (such as sand), mixed with water, without connotation as to composition" (AGI, *Glossary of Geology*, 1972).

bidites it was tacitly assumed, or sometimes argued, that most or all of the pelitic layers represent the normal, pelagic settling, interrupted at times by the instantaneous emplacement of turbidite sands (e.g., Sujkowsky, 1957; Dzulynski, Ksiazkiewicz, and Kuenen, 1959; Gorsline and Emery, 1959; Stanley, 1963). More recent studies of turbidite sequences have also implied that the pelitic layers represent normal, pelagic settling (e.g., Cline, 1970; McBride, 1970; Moore, 1971).

However, during the past decade or so the conviction has been growing that at least a portion of the mud layers in the modern deep sea is deposited by turbidity currents. Van Straaten (1966, 1967, 1970) recognizes turbiditic mud layers in the southern Adriatic Sea. Van Andel and Komar (1969) document resedimentation by turbidity currents of pelagic oozes in valleys on the flanks of the Mid-Atlantic Ridge. A considerable fraction of the thick, largely muddy wedges forming base-of-slope deposits are also deposited by turbidity currents (Stanley, 1969, 1970). Piper (1973) describes silts and muds of turbiditic origin from the Gulf of Alaska.

Evidence that at least part of the pelitic division (*e*) is turbiditic in origin is provided mainly by the faunal content. Instances have been found in which only the upper part of the pelitic layer contains a relatively high percentage of skeletal remains of pelagic and deep benthonic organisms (Ksiazkiewicz, 1961; Natland, 1963; van Hinte, 1963; Weidmann, 1967; Weiler, 1967; Comas, 1968; Davies, 1968; Tanaka, 1970; and others). This upper part of the pelite is, in several of these instances, of a different lithology and color (Ericson, Ewing, and Heezen, 1952; Bornhold and Pilkey, 1971; Huang and Pierce, 1971). Graptolites in the pelite have been shown to be oriented parallel to the sole markings of the underlying turbidite sandstones (Moores, 1969). Textural evidence for turbidite deposition, such as grading in the lower part of the pelitic layer, and grading throughout the entire pelite division, have been found as well (Radomski, 1958, 1960; Piper, 1972; Rupke, 1972; Hall and Stanley, 1973). Other evidence for the turbiditic origin of pelites comes from various statistical analyses of bed-thickness properties (Enos, 1969; Rupke, 1969).

In some publications the pelitic division has been regarded as almost entirely turbiditic, with little or no pelagic sediments forming the top part (Nesteroff, 1961; Bouma, 1962; Nesteroff and Heezen, 1963; Rusnak and Nesteroff, 1964).

In their reviews of ancient and modern flysch-type sequences, Dzulynski and Smith (1964) and Kuenen (1964) concluded that in flysch-type sequences the pelites are dominantly turbiditic in origin, and that the truly pelagic parts are insignificant in volume. In a number of publications it has simply been assumed that some (lower) parts of the pelitic layers are turbiditic, while other (upper) parts are pelagic, without specification of criteria (Nederlof, 1959; Holtedahl, 1965; Walker, 1967; and others).

In recent years, other depositional mechanisms for fine-grained sediments have been proposed, in addition to pelagic settling and turbidity currents. Ewing and Thorndike (1965) observed a nepheloid layer of suspended fine-grained sediment on the continental slope and rise of northeastern America, which may play a role in resedimentation of muds. Similar low-density and gravity-assisted flows carrying fine-grained sediments to deep marine environments have been proposed. These can be of permanent nature or can be seasonally reactivated during river flooding or scouring of the outer shelf margin by storms (Moore, 1969; Bartolini and Gehin, 1970; Stanley, Gehin, and Bartolini, 1970; Stanley, Sheng, and Pedraza, 1971; Fleischer, 1972; Huang and Stanley, 1972).

Normal bottom currents, in particular geostrophic contour-following currents (Heezen, Hollister, and Rudiman, 1966), are thought to play a role as well in deep-sea sediment transport and deposition. Deposits by these currents, called contourites, are described by Wezel and Ryan (1971) and Bouma (1972a, 1972b) in ancient flysch sequences; Bouma (1972a, 1972b) tabulates the differences between turbidites and contourites. These bottom currents are capable of reworking sands (Hubert, 1964), but are invoked mainly for the transport and deposition of very fine sand and silt.

In summary, there is evidence for several depositional mechanisms affecting fine-grained sediments in both modern and ancient deep marine environments. The question, however, of how much of the pelitic layers in turbidite sequences is accumulated by pelagic settling, and how much by turbidity currents, bottom currents, or other depositional mechanisms remains largely a matter of doubt and

dispute. The present study addresses itself to this question of the origin of mud layers and constitutes an attempt to define, from an analysis of different types of mud, criteria that may indicate a particular mechanism of deposition. This investigation has been carried out using sediment cores from the southern part of the Balearic Abyssal Plain in the western Mediterranean.

Recognition of the depositional mechanisms of deep-sea muds is not only of significance for the understanding of deep marine processes of sediment distribution, but is also essential for studies of the chronology and paleoclimatology of deep-sea cores.

ACKNOWLEDGMENTS.—We are indebted to the U.S. Navy for providing shiptime and facilities aboard the USNS *Lynch* on its cruise (LY–II–72) in March-April 1972, and for furnishing the cores and 3.5 kHz records used in this study. In particular, we thank the officers and crew of the *Lynch,* and scientific personnel including students from Williams College and the University of Illinois for their assistance aboard ship. Mr. Harrison Sheng, Smithsonian Institution, assisted with various laboratory analyses. The paper has been critically read by Drs. A. G. Fischer, Princeton University, H. G. Reading, Oxford University, and L.M.J.U. van Straaten, Rijksuniversiteit, Groningen; we appreciate their constructive criticisms and suggestions. Funding for this study, part of the ongoing Mediterranean Basin Project, was provided by the Smithsonian Research Foundation grant (DJS) FY73-430035. This investigation was undertaken while Rupke held a postdoctoral fellowship at the Smithsonian Institution.

Geographic and Geologic Setting

The Balearic Sea, also referred to as the Algéro-Provençal Basin, occupies most of the western Mediterranean. It extends from the Ligurian Sea in the northeast and the coast of southern France in the northwest, southward between Corsica-Sardinia and the Balearic Islands, down to the coast of North Africa. Cores examined in this study were collected in the southern part of the Balearic Sea, known as the Algéro-Balearic Basin (Figure 1). The present geographic configuration has been explained in terms of rifting, lateral spreading, and rotation of microblocks (Iberia, the Balearic block, and the Corsica-Sardinia block) (Ritsema, 1969; Hsü, 1971; Vogt, Higgs, and Johnson, 1971; Auzende, Bonnin, and Olivet, 1973; Dewey, et al., 1973). In addition to lateral spreading, evidence for vertical tectonics has been presented (Bourcart, 1959; Pannekoek, 1969; van Bemmelen, 1969).

The Balearic Basin is bounded by narrow shelves, platforms, and continental slopes that, for the most part, exceed 5°. These are in many places incised by submarine canyons (Bourcart, 1959). They border a large, flat basin floor, called the Balearic Abyssal Plain, the largest basin plain in the Mediterranean Sea. The 2600 m bathymetric contour serves to delineate the abyssal plain (Carter et al., 1972).

The plain, a depositional feature, forms the surface of a stratified sedimentary fill, of which the thickness is estimated from subbottom profiles at 300 to 450 m (Horn, Ewing, and Ewing, 1972). The total thickness of the Plio-Quaternary unconsolidated sediment fill reaches to 1200 m in the vicinity of the Rhône Cone (Menard, Smith, and Pratt, 1965; Watson and Johnson, 1969; Ryan et al., 1969). Piston-coring surveys show that the sediment underlying the plain comprises mostly mud with some alternating graded and laminated sands and silts. JOIDES drilling in the Balearic Basin (Leg 13, sites 124, 133, 134) reveals thick deposits of Quaternary and Pliocene age, underlain by a Messinian evaporite sequence (Ryan, Hsü, et al., 1937a,b). For instance, at site 124 situated off the eastern margin of the Balearic rise (Figure 1), a thick sequence of rhythmically bedded sediments has been recovered. Its lower part (200 m), largely of Pliocene age, contains light- and dark-colored marl oozes and sand-silt laminae, which form the bases of the dark oozes. The upper part (160 m), of Quaternary age, contains alternating graded sand-silt layers and marl oozes. Nesteroff (1973) and Nesteroff, Wezel, and Pautot (1973) interpret the lower section as contourites, and the upper section as turbidites (cf. Nesteroff et al., 1972).

The abyssal plain surface has a slight gradient away from the main source of terrigenous sediment and toward its deepest part (2800 m) lying west of Sardinia. The most important terrigenous sediment source is the river Rhône, the mouth and submarine fan of which are located in the northwestern part of the basin (Menard, Smith, and Pratt, 1965; Horn, Ewing, and Ewing, 1972). The

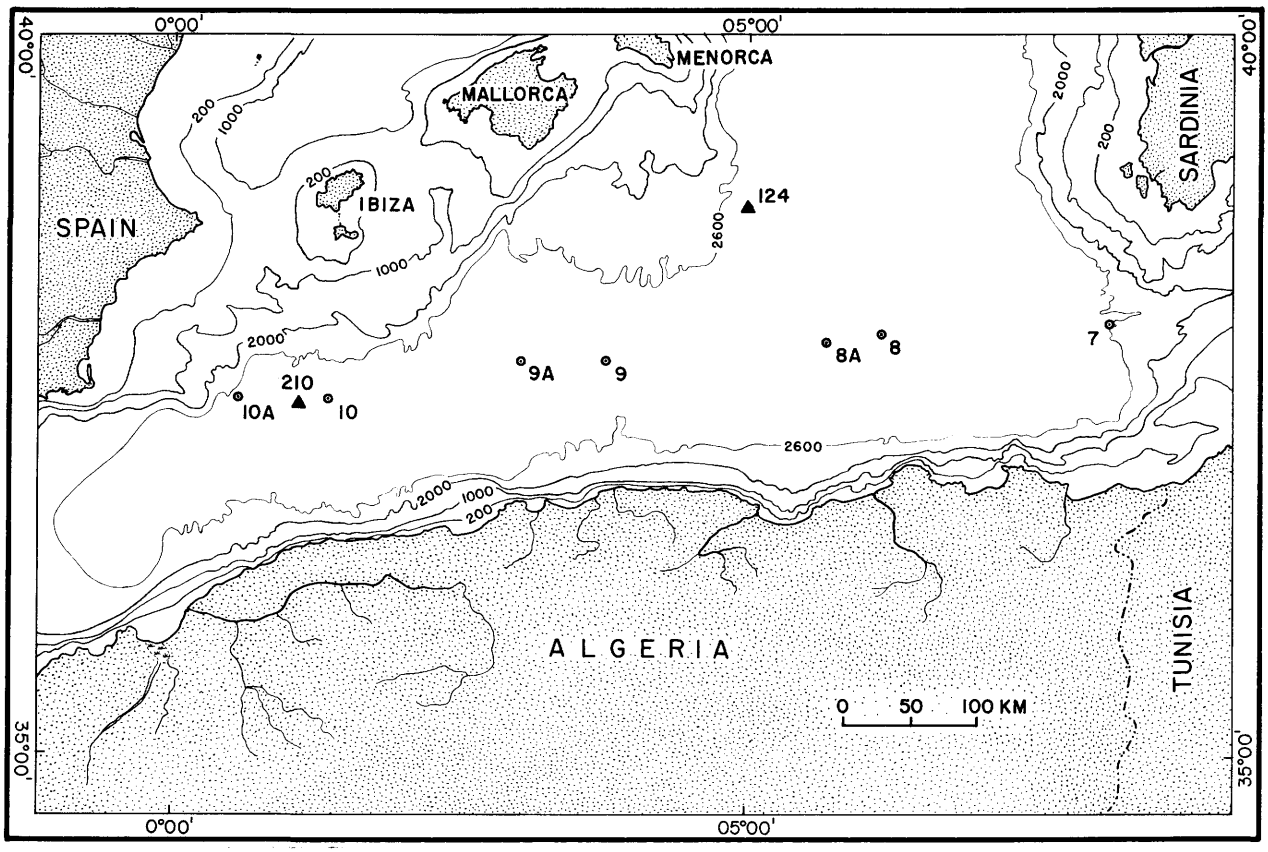

FIGURE 1.—Locations and numbers of seven cores taken from the Balearic Abyssal Plain during March-April 1972 aboard the USNS *Lynch*. The isobaths are in meters. The 2600 m isobath delineates the abyssal plain. JOIDES leg 13 site 124 and core 210 of the Swedish Deep-Sea Expedition are also shown.

Rhône has been the main source of sediment since the Pliocene foundering of the northern Mediterranean margin (Bourcart, 1959), and probably earlier. Another important source of fluvial sediments is the North African margin (Leclaire, 1972a, 1972b; Vita-Finzi, 1972); much of these materials bypass the narrow shelf and move downslope, in some cases via canyons, toward the plain surface. To a lesser degree, sediments are also derived from the Iberian Peninsula, the Balearic Platform, and the Strait of Sicily. River input is to a large degree seasonally controlled; late fall to spring rains and snow-melt result in increased discharge during these periods (Semple, 1931). Seasonally shifting wind patterns also modify the volume of aeolian dust transported off the North African margin (Eriksson, 1965).

The movement of the upper two water masses [surface and intermediate or Levantine water (Wüst, 1960; Lacombe and Tchernia, 1972)] are influential in the movement of fines and planktonic organisms in suspension. Little is known of bottom water flow and velocities (Miller 1972). Bottom photographs made in this region do not indicate evidence of significant bottom current activity. The role of large-scale vertical sinking of surface water in the northern Balearic Sea (Stommel, Voorhis, and Webb, 1971) as a significant mechanism in sediment transport to the basin plain has yet to be evaluated.

Earthquakes play an important role in triggering turbidity currents, slumps, and other mass gravity failures along the steep, narrow margin of this region. The area is seismically active (Bara-

zangi and Dorman, 1969; McKenzie, 1970); a line of earthquake epicenters trends from the Azores to the Strait of Gibraltar eastward across North Africa to Sicily. The Orleansville earthquake of 1954, for instance, triggered a large turbidity current in the southwestern sector of the Algéro-Balearic Basin, an occurrence well documented by cable breaks (Heezen and Ewing, 1955; Horn, Ewing, and Ewing, 1972).

The structural mobility of the region also affects sedimentation in other ways. Numerous salt dome diapirs (Watson and Johnson, 1969; Ryan et al., 1969) of Messinian age (Ryan et al., 1973) occur across much of the abyssal plain. Salt tectonics has disturbed the Quaternary sediment succession, including the uppermost Holocene strata in many places, particularly in the vicinity of 2° longitude (Stanley and Diester-Haas, 1973). Elongate salt knolls deflect sediment dispersal along the plain surface and locally act as dams against which stratified deposits are ponded (Figure 2).

Core Locations

During the March-April 1972 cruise of the USNS *Lynch* (LY–II–72), seven Ewing piston cores were retrieved from the Balearic Abyssal Plain at seven different stations in the Algéro-Balearic Basin. The cores are coded from east to west LY–II–7, –8, –8A, –9, –9A, –10, –10A (Figure 1). Stations were selected for deepwater light scattering experiments, and not with a sedimentary basin analysis in mind. The cores, therefore, constitute random sediment samples from the Balearic Abyssal Plain.

TABLE 1.—*Location, water depth, and length of seven cores obtained from the Balearic Abyssal Plain on the USNS* Lynch *March–April 1972 cruise (see Figure 1)*

Core no.	*Latitude*	*Longitude*	*Water depth* (*m*)	(*fm*)	*Core length* (*cm*)
7	38°02.7′N	8°09.2′E	2588	(1415)	342
8	37°58.8′N	6°11.0′E	2719	(1487)	428
8A	37°56.0′N	5°41.0′E	2712	(1483)	382
9	37°47.3′N	3°43.0′E	2674	(1462)	513
9A	37°47.0′N	3°00.9′E	2676	(1463)	444
10	37°31.1′N	1°18.9′E	2655	(1452)	445
10A	37°32.0′N	0°33.5′E	2628	(1437)	461

The ship track, along which almost continuous 12 and 3.5 kHz echo-sounding records were obtained, extends from the western sector of the Strait of Sicily to the region south of the Balearic Islands and the southeastern coast of Spain in the vicinity of the Mar Menor. This east-west trending line constitutes an almost complete section across the Algéro-Balearic Basin, and is oriented approximately at right angles to the main directions of sediment supply (except for cores 7 and 10A).

Core location, length, and uncorrected water depth are listed in Table 1. Total core lengths range from 342 to 513 cm; the average core length is 431 cm. The water depth ranges from 2588 to 2719 m. The position of cores 8 to 10A, as indicated on echo-sounding records, is shown on Figure 2.

Core LY–II–7 was collected on the lower fan surface of the Strait of Sicily Fan, just south of a levee bounding the southern margin of the Strait of Sicily Canyon.

Core LY–II–8 was retrieved on the almost horizontal basin plain surface, while LY–II–8A was cored in a wedge of stratified sediment ponded behind an emerged salt dome.

Cores LY–II–9, –9A, and –10 were collected in a zone of distinctly stratified sediment between salt domes south of the Balearic block; evidence of salt tectonism such as rim synclines, arching of strata, faults, and grabens occur in the immediate vicinity.

Core LY–II–10A was retrieved east of the Mazzaron Escarpment and just beyond the Mar Menor Fan; the plain surface has a low gradient, and lies in a structurally active region in the westernmost Algéro-Balearic Basin.

Lithologic Description of Cores

General

The seven cores consist predominantly of muddy sediments. Visual examination of split cores shows that much of the core sections appears homogeneous (Figure 3). Lamont-Doherty cores taken in the same general area have been interpreted as consisting largely of homogeneous mud (Horn, Ewing, and Ewing 1972). In most of the cores, a few sand-silt and silt intercalations stand out as a result of textural and color differences (Figure 3).

The cores were initially cut in 2 m sections and

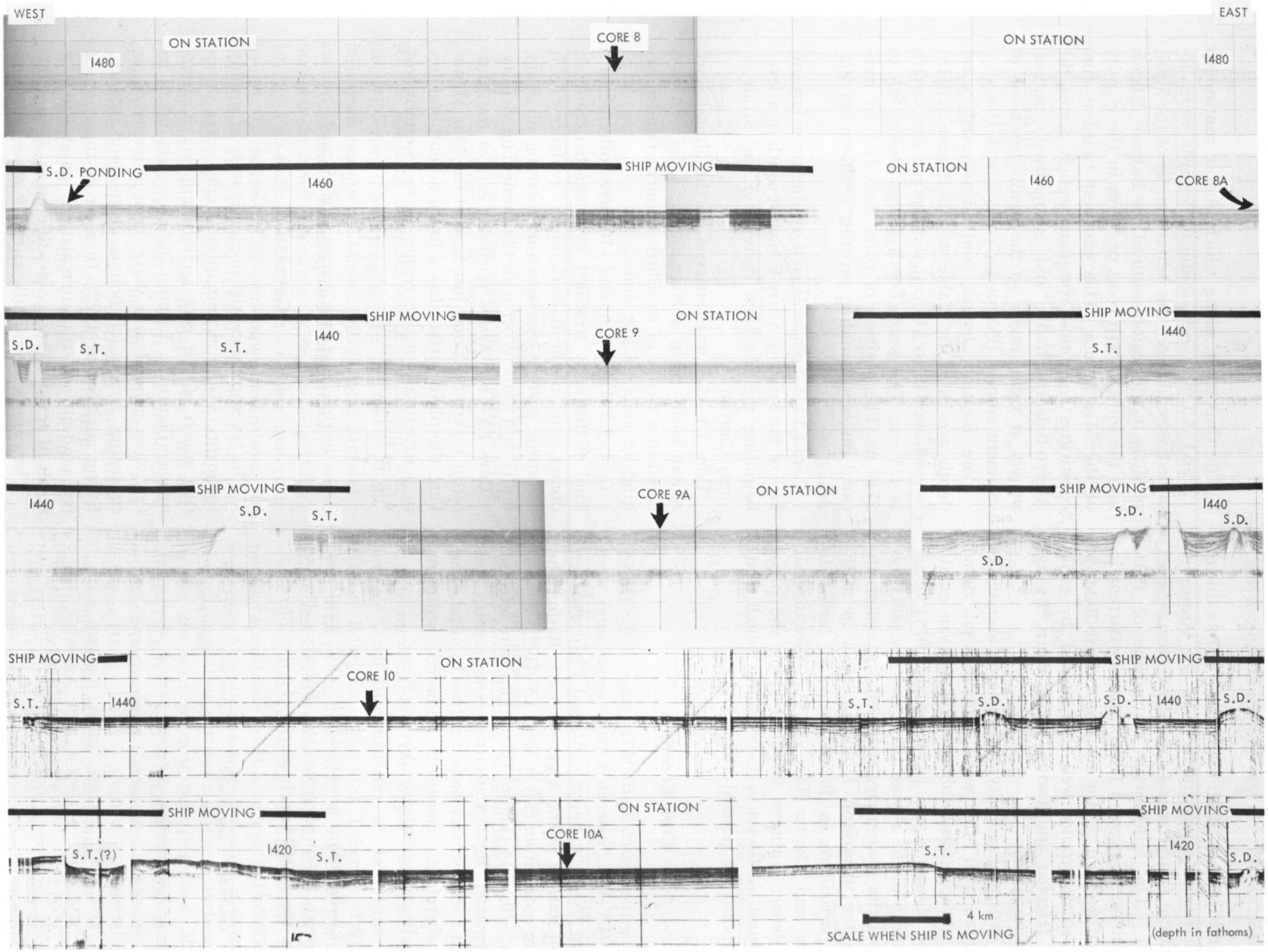

FIGURE 2.—High resolution 3.5 kHz subbottom reflection profiles of the sea floor in the vicinity of core locations 8 to 10A. (S.D. = salt doming. S.T. = salt tectonics.)

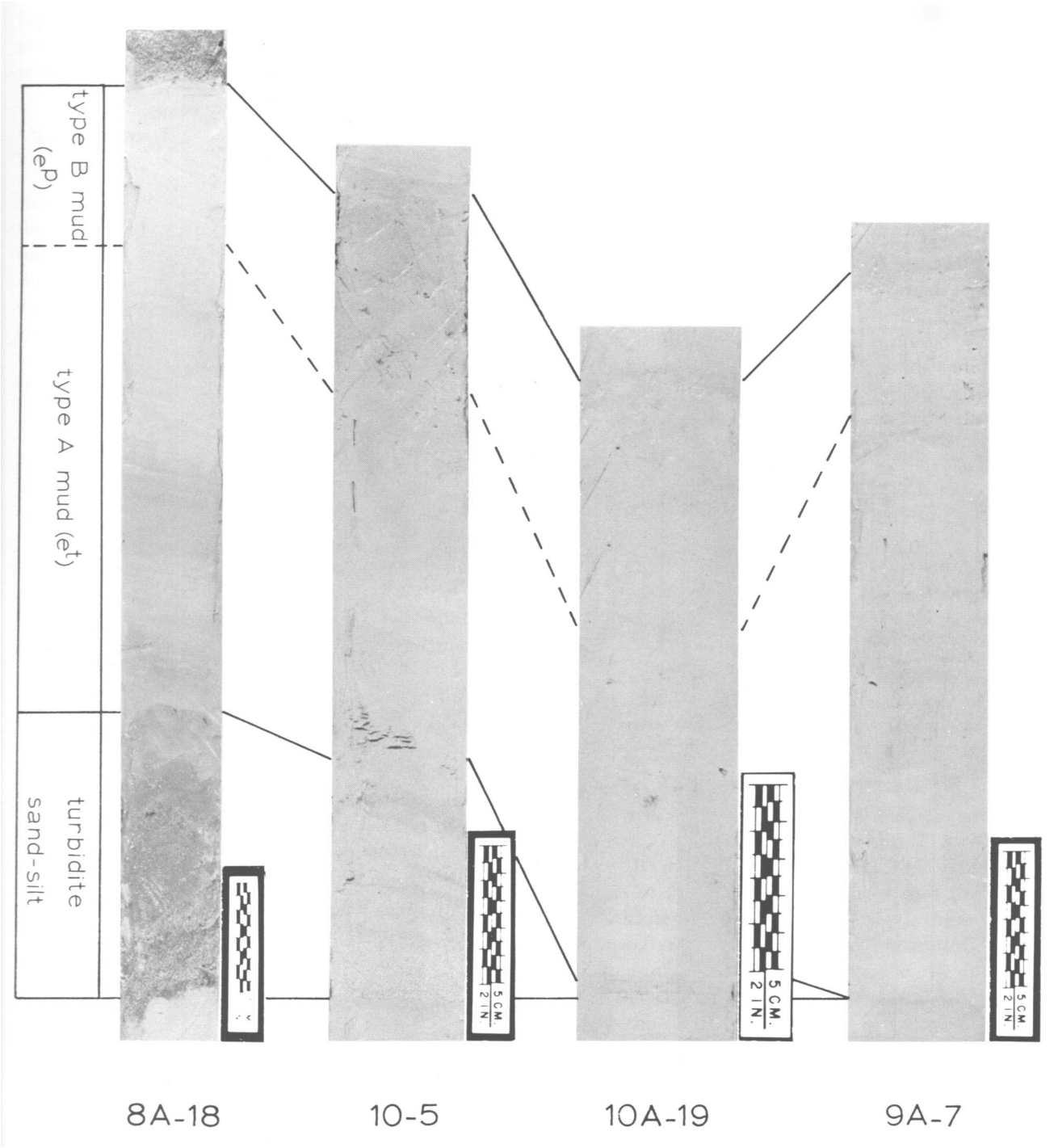

FIGURE 3.—Photographs of split-core sections containing typical successions of turbidite sand-silt layers (8A–18, 10–5) or silt laminae or lamels (10A–19, 9A–7), and two types of mud layers, A (e^t) and B (e^p). Note the absence of clearly visible layer boundaries within the muds. The interpretative column on the left is largely based on X-radiographs of these sections. The first part of the section numbers refers to a core, the second to a rhythm within a core.

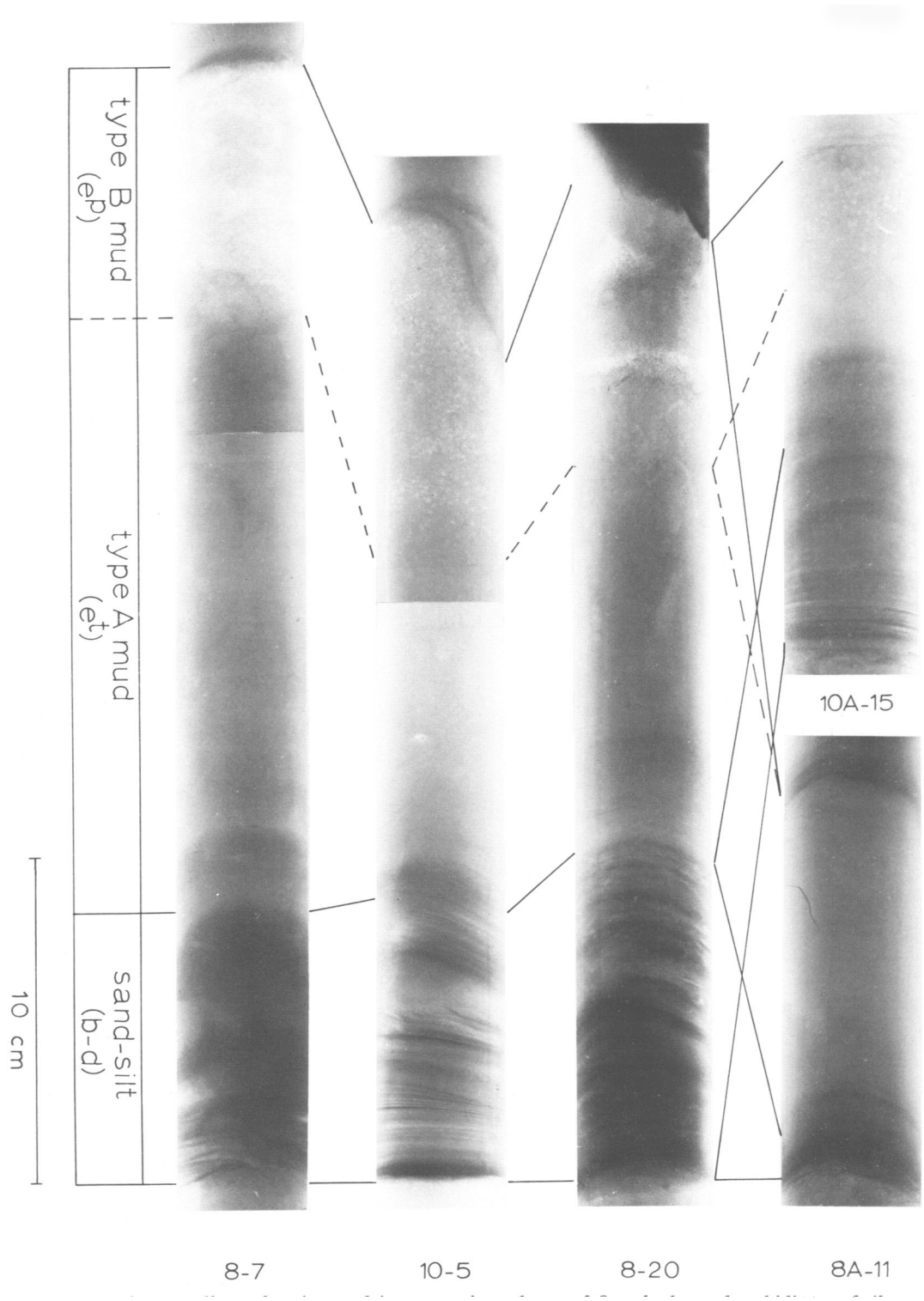

FIGURE 4.—X-radiograph prints and interpretative column of five rhythms of turbidite sand-silt layers or silt laminae, followed by largely homogeneous type A mud (e^t), which in turn is followed by type B mud (e^p) exhibiting light speckling. The lower part of type A layers can be finely laminated (10–5, 8–20, 10A–15). One rhythm (8A–11) contains no type B layer. In the turbidite sand-silt layer in rhythm 10–5, note current ripple lamination between two co-sets of lower and upper parallel lamination. Also note in type B mud layer two horizons of extra light speckled bands. The distinct horizontal lines in 8–7 and 10–5 are artifacts produced by the joining of two different photographic prints.

kept in cold storage, split, color logged, photographed, and X-radiographed before sediment samples were taken for detailed analysis.

X-RADIOGRAPHIC IDENTIFICATION OF MUD LAYERS

The X-radiographs of split-core sections reveal that the sand-silt and silt layers exhibit several of the structural characteristics associated with turbidites. All layers are base-cutout successions of Bouma divisions, viz., T_{b-c-d}, T_{c-d}, or T_d (Figure 4). The lowermost graded *a*-division is never present. The base of these layers is sharp, and fining-upward grading is macroscopically visible in the split cores. These layers are interpreted as typical turbidite sands or silts.

In addition to these turbidite sand-silt layers, the X-radiographs reveal a large number of distinct mud layers, many of which are very difficult to recognize in the split cores (Figure 3). These more subtle layers overlie sand-silt turbidites, or they begin with a dark line on X-radiograph prints, constituting silt laminae (less than 1 cm thick) or lamels (less than 1 mm thick). The lower boundary of the coarser grained lower laminae or lamels is always sharper defined than the upper. Two kinds of mud occur above these layers, as well as on top of the turbidite sand-silt layers. *Type A mud,* which appears darker, lies directly on top of the coarser layer below. Its lower portion can exhibit delicate lamination. *Type B mud* appears lighter and is distinguished by light specks; it lies on top of type A mud and precedes the coarser layers (Figure 4). The speckling is produced by interspersed microskeletons of foraminifera and pteropods in the mud.

The boundary between mud types A and B is often gradual and in some instances blurred by mottling and other evidence of bioturbation. The upper portion of type A mud layers can contain tubes consisting of FeS_2 (Figure 18F). Such pyritized filaments are reported by Hesse and von Rad (1973) in sediments from the Strait of Otranto. These, readily apparent in X-radiographs, probably result from burrowing organisms.

Delicate and sometimes repeated scraping of the wet sediment surface of the split cores is necessary to observe the boundaries of the mud layers identified in X-radiographs. As can be seen from a comparison of core section 10–5 illustrated in Figures 3 and 4, many of these lithologic boundaries would go unnoticed without the aid of X-radiographs.

VARIATIONS WITHIN CORES

Vertical variation within the cores consists of a rhythmic succession of three members, viz., (1) the coarser grained turbidite sand-silt layer, or the silt lamina or lamel, (2) the type A mud layer, and (3) the type B mud layer. A unit consisting of any of the three members is herein called a *rhythm.* In some rhythms the lower coarser grained member is absent, or the upper type B mud member is missing, or both. In general, four types of rhythmic successions of the three members occur in the cores (Figure 5).

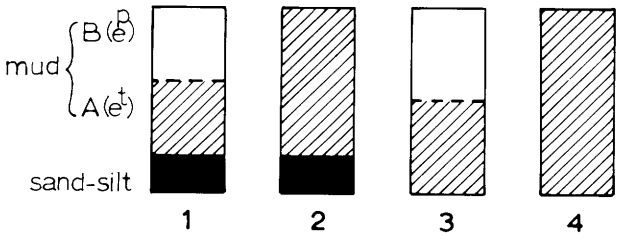

FIGURE 5.—Four types of rhythmic successions of three member layers (sand-silt, and two types of mud) as found in seven cores from the Balearic Abyssal Plain (see Figure 6).

The average thickness of turbidite sand-silt layers is 4.5 cm; of type A mud layers 17.5 cm; and of type B mud layers 10.5 cm. The maximum thickness of type A mud is 47.5 cm, and the minimum thickness 1 cm. For type B mud, these values are respectively 53.5 cm and imperceptibly thin. The measuring accuracy varies, but is approximately 0.5 cm for the mud layers and can be 0.1 mm for the sand-silt layers.

VARIATIONS BETWEEN CORES

The sand-silt or silt members, type A muds, and type B muds are depicted in Figure 6; thickness data are listed in Table 2. The cores contain widely varying numbers of rhythms, viz., from cores LY–II–7 to 10A respectively: 25, 23, 22, 12, 18, 13, and 25. Their average thicknesses vary accordingly (Table 2; Figure 6).

TABLE 2.—*Number, thicknesses (in cm), and thickness statistics of sand-silt turbidites (Sa-Si), type A mud layers (interpreted as turbiditic or e^t, and type B mud layers (interpreted as hemipelagic or e^p), in seven cores (7–10A) from the Balearic Abyssal Plain (the layer succession is listed from left to right, and upward, in each core column)*

	7			8			8A			9			9A			10			10A		
Rhythm No.	Sa-Si	(e^t)	(e^p)	Sa-Si	(e^t)	(e^p)	Sa-Si	(e^t)	(e^p)	Sa-Si	(e^t)	(e^p)	Sa-Si	(e^t)	(e^p)	Sa-Si	(e^t)	(e^p)	Sa-Si	(e^t)	(e^p)
26																			2.5	5.5	42.5
25	0.2	5																		5.5	
24	0.2	10.5	3.5	3.5															2	9	0.5
23		8.5	5	16	8															2	11
22	0.2	6	5.5		14.5		7	19											5	11.5	12.5
21	0.4	11		12	6	2		13.5												4	
20		3	2	10	11.5	8.5		9	2.5										0.3	15.5	53.5
19		4	3	13	16.5	6.5	8	13.5	3.5					5	16				0.5	9.5	6.5
18		4	9.5		7.5		14	21	7.5					10	14.5					3	3.5
17	0.3	5.5	38	2.5	8	5		12	3					9	25.5					2	2
16	0.2	8	15		6.5	1	5.5	7.5	3.5				4	11	1					1	5.5
15		5.5	23	1	10	3.5	8	9.5	3.5					8.5	23				6	5	4
14	0.2	3.5	11	4	6.5	3		8	9					20.5	3		21	26		4	3.5
13		10	9	8	14			12	7.5				0.5	45	8.5	1.2	12	29		9	7.5
12		8.5	2.5		9.5	4.5	0.7	13	3.5		11.5	44.5	2	17	6.5	11	11.5	1		1.5	6.5
11	0.2	5	44.5	0.3	17.5	14	1.5	10			16			10	17.5	7.5	13.5	16	33.5	12	16
10	0.2	4			1			10.5	6	0.7	17	18		4	27.5	9	23.5	9		2.5	
9	0.5	3	3.5		10	7	10.5	12	5	0.2	45	7.5	2	6	2.5	0.2	35.5		1	3	1.5
8		1		3	13	3	0.7	10.5	6	3	41.5	5		12	2		28	4		18	3
7	0.3	4.5	16	8.5	17.5	8	5.5	16.5	1		17	38		21.5	5.5		24	25.5	2	1.5	3.5
6		3	6		1.5	14.5		1			18.5	12.5	0.4	13.5	4	4	18.5	23.5	0.8	7	7.5
5	0.2	2			1		18	11	4.5		22	5	0.3	23	1	8.5	10.5	7	0.3	2.5	1
4	0.2	2	6	10	13	5		11.5	2	0.8	45.5	3.5	0.5	23.5	2.5	2.5	15.5			2	23
3		2	1.5	2.5	10	3	7	1			13	36		2	12	1.5	14	5.5	0.4	1	4.5
2	0.1	5.5	8		7.5	2.5	0.7	1.5		7	47.5			13	4.5	3	15	2.5	1	4	31
1		2			21	11		1		26	10.5				3			5	55.2		14
Average thickness	0.2	5	11	6.7	10	6	6.7	10.5	4	6.3	25.5	19	1.4	14	9.5	4.6	18.5	13	4.7	5.5	11.5
% of total thickness	1	37	62	22	54	24	23	59	18	7	60	33	2	58	40	10	55	35	12	31	57

The ratios of the three different members change markedly from core to core, across the Algéro-Balearic Basin. These changes correlate roughly with water depth. This is schematically represented in Figure 7, where the proportions of the different sediment types (B) are plotted along a bathymetric profile (A) from station 7 to station 10A. In cores at greater depth (8 to 10) the proportion of type A mud is more than 50 percent. In cores at shallower depths (7 and 10A) the percentage of type B mud is more than half (Table 2).

Another possible correlation is to be noted, viz., between lithology and access to fluvial sediment sources. Cores 8, 8A, 9, and 9A occupy positions north of the important oueds on the margin of North Africa (Figure 1).

COLOR OF SEDIMENT

The sand-silt turbidites, when terrigenous in composition, are olive gray (5Y 4/1) in color. Bioclastic layers are yellowish gray (5Y 7/2). Type A mud is light olive gray (5Y 5/2) to dusty yellow (5Y 6/4), whereas type B mud is somewhat lighter in color, namely, light olive gray (5Y 6/1) to yellowish gray (5Y 7/2). Color differences have been used to define mud layers (Bornhold and Pilkey, 1971; Davies, 1968; Fleischer, 1972; and others).

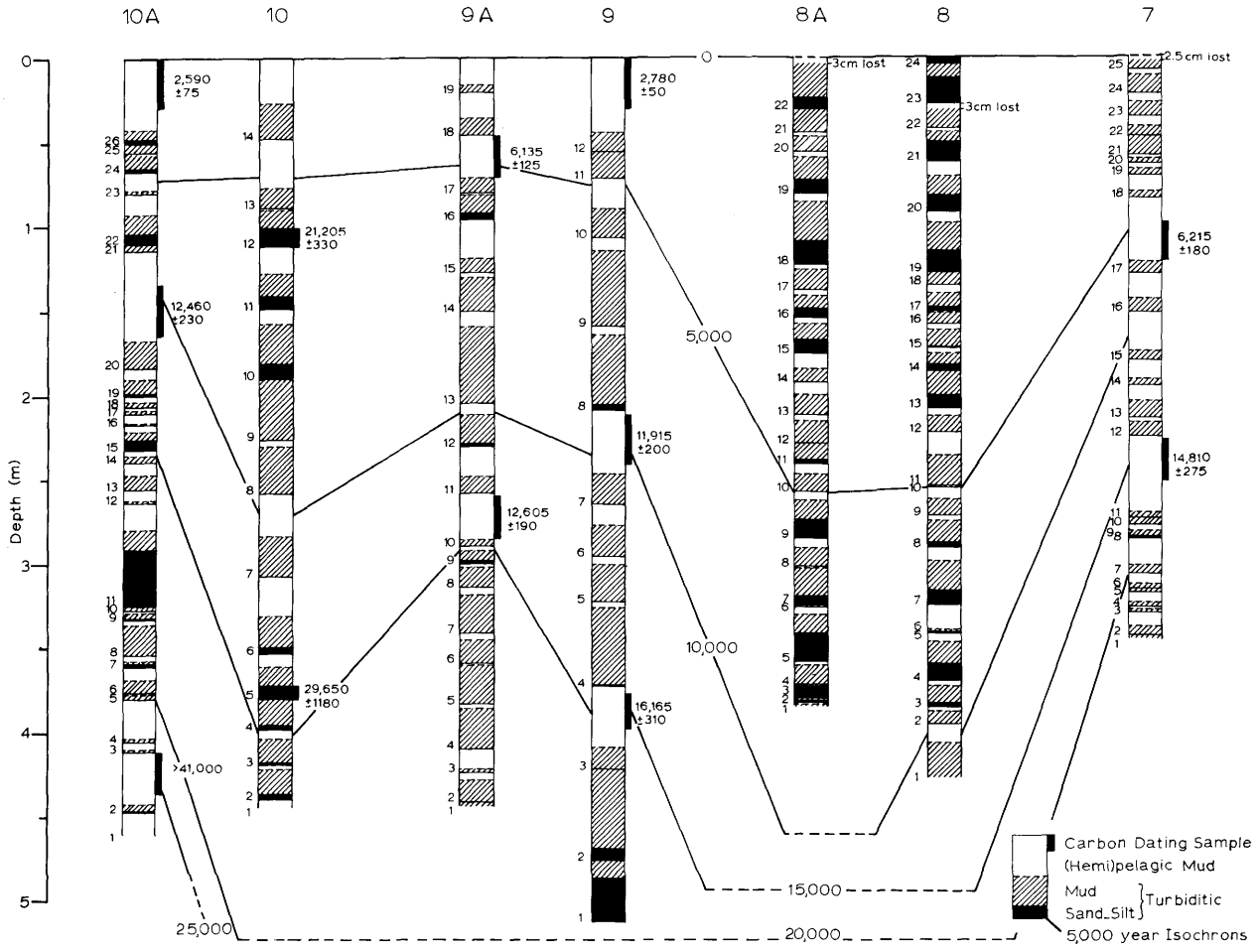

FIGURE 6.—Distribution of rhythms (numbered on left side of cores) consisting of turbidite sand-silt layers and two kinds of mud layers, type A (interpreted as turbiditic) and type B (interpreted as hemipelagic) in seven cores from the Balearic Abyssal Plain. Spacing between these cores corresponds to the distances between their respective locations. The position and extent of samples for radiocarbon dating and the corresponding ages are indicated. Isochrons are drawn between the cores, based on a calculation of the hemipelagic rate of sedimentation. Note that in core 10 the radiocarbon dates are determined not on type B muds (interpreted as hemipelagic), but on resedimented turbidite sands, causing a dicrepancy between these dates and the ages indicated by the isochrons.

However, a comparison of color logs with X-radiography data shows that color is not a reliable boundary criterion. Color changes in the cores often do not coincide with layer boundaries, particularly the boundaries between type A and type B layers. The boundary area can display mottling or can be uniform in color. A distinct color change is present within the type A mud member, some 15 cm below its boundary with type B mud in rhythm 18 of core 8A (Figure 3). Such discrepancies may be the result of burrowing activity.

Analysis of Rhythms

GENERAL

Eight individual rhythms were selected from six of the cores (7, 8, 8A, 9A, 10, 10A) for detailed sampling and analysis. The main purpose of the analysis was to establish and to contrast the properties of mud types A and B in order to gain insight into their mode of origin. The rhythms are labeled by the number of the core and the number of the rhythm within that core. The following rhythms

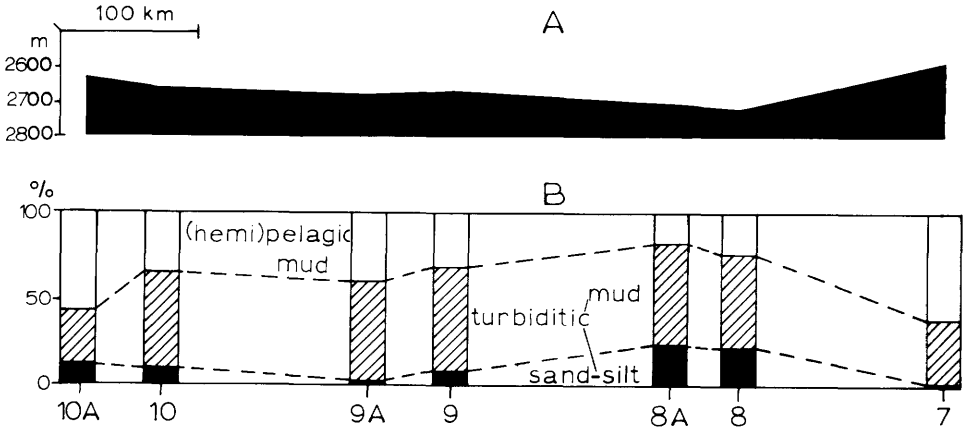

FIGURE 7.—A, An east-west schematic bathymetric profile across the Balearic Abyssal Plain from station 7 to 10A. B, Proportions of total turbidite sand-silt (black), total type A mud (hatched; interpreted as turbiditic), and total type B mud (white; interpreted as hemipelagic). Note the rough correlation between water depth and proportion of turbidite sand-silt-mud.

were selected: 7–11, 8–7, 8A–11, 8A–18, 9A–7, 10–5, 10–12, and 10A–19.

The rhythms were selected so as to represent variety in terms of spread between the cores, spread within the cores, thickness of the rhythms, thickness of the rhythm members, and type of rhythm. The thickness of the sampled rhythms ranges from 11.5 cm (8A–11) to 49 cm (7–11); the average thickness is 29 cm. The average thickness of type A mud layers is 13 cm and that of type B layers 10 cm (Table 3). All four types of rhythms (Figure 5) are represented. Two have a thick type A mud member (8A–18, 9A–7), and one has a thick type B mud member (7–11) (Table 3).

TABLE 3.—*Thickness (in cm) of eight individual rhythms of sand-silt turbidites, type A (e^t) and type B (e^b) muds, which were selected for detailed sampling and analysis*

Core no.	*Rhythm no.*	*Sa-Si*	*A (e^t)*	*B (e^b)*	*Total*
7	11	0.2	5	44.5	49.2
8	7	8.5	17.5	8	34
8A	11	1.5	10	0	11.5
8A	18	14	21	7.5	42.5
9A	7	0	21.5	5.5	27
10	5	8.5	10.5	7	26
10	12	11	11.5	1	23.5
10A	19	0.5	9.5	6.5	16.5
Average thickness		5.7	13	10	28.8

ANALYTICAL PROCEDURES

Samples were taken from the split-core halves. The sample thickness ranges from 3 to 8 mm. The distance between samples varies from 0.5 to 8 cm. A total of 59 samples has been analyzed. For the study of clay mineralogy, four extra samples were selected.

The selection of exact sample points was based on the structural and textural details provided by the X-radiographs of the rhythms. The advantage of this sampling technique is that no subtle changes in sediment structure or texture were overlooked. It also makes possible a more precise correlation between the sedimentary structures of the sediment sections and the results of the textural and compositional analyses.

The following analytical procedures were carried out on all samples: (1) a grain-size determination by pipette analysis; (2) a determination of carbonate percentage by gravimetric ascarite absorption; (3) a compositional analysis of the sand fraction of all samples by grain-mount counting; (4) a study of the overall composition, and in particular of the clay mineralogy, by X-ray diffractometry and peak-height analysis.

The results are presented for each rhythm separately (Figures 8–15). Each figure is composed of five columns, the first of which provides the sedimentary structures (Bouma divisions) based on the X-radiographs. In this column the lower mem-

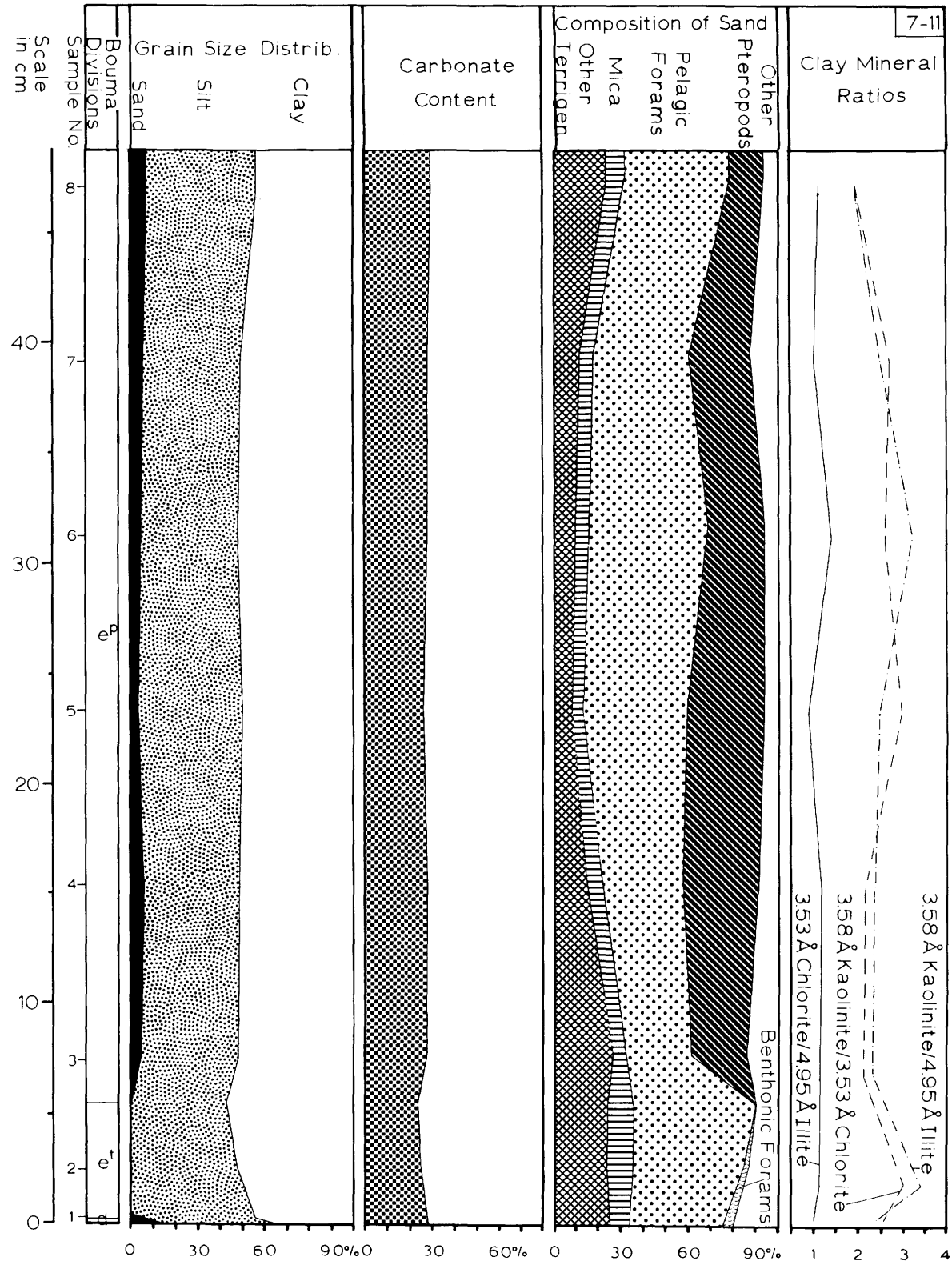

FIGURES 8–15.—Diagrammatic summaries of the sedimentary structures and textural and compositional properties of eight rhythms from six cores from the Balearic Abyssal Plain. The coarse-grained material in the top part of rhythm 8A–11 may be due to burrowing from above rather than representing a separate type B mud layer. Sample numbers marked with "a" and "b" were used only in the study of clay mineralogy.

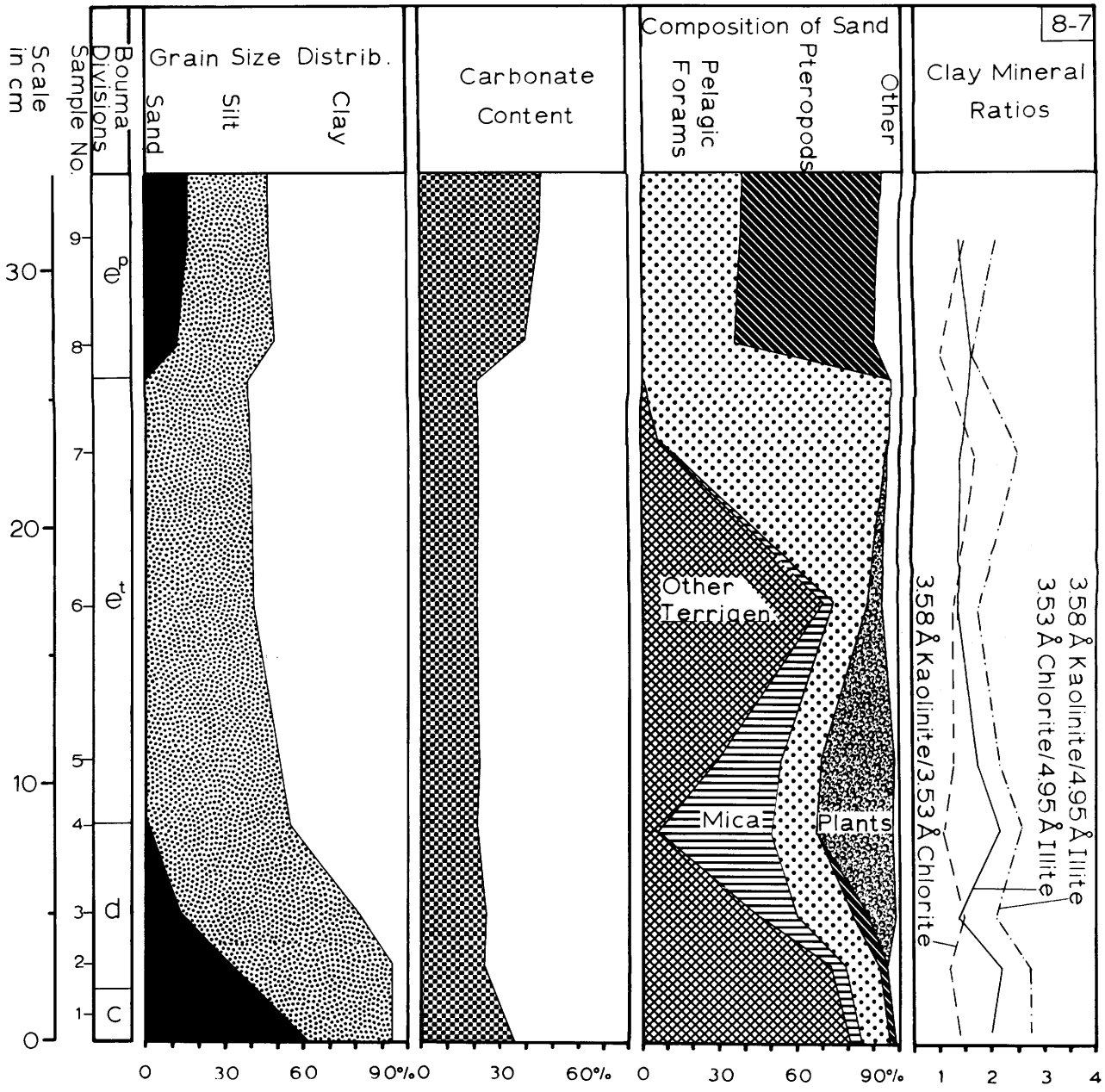

FIGURE 9.

ber of each rhythm (turbidite sand-silt layer or silt lamina) is indicated by Bouma divisions *b*, *c*, and *d*, while in anticipation of their genetic interpretation the middle (type A mud) and upper member (type B mud) are indicated by e^t and e^p respectively. In the three following columns, sample points have been connected by straight lines, except where they lie on both sides of the mud A-B boundary. Where in X-radiographs this boundary is clearly defined, the lines are extrapolated from above and below and display the changes of texture and composition in the boundary region.

Grain-Size Distribution

The grain-size distribution of the eight rhythms has been determined by pipette analysis. Measurements were taken at 1 phi intervals, between 4 phi and 9 phi (63 and 2 microns respectively). Type A mud contains less than 1 percent sand; thus, no size analysis of the coarser than 4 phi fraction was made. The terms "sand," "silt," and "clay" are used as grain-size terms without any compositional connotation.

The results are grouped and plotted in two different ways. (1) The percentages of sand (larger than 63 micron), silt, and clay (smaller than 2 micron) (Table 4) are plotted against sample point positions within rhythms (Figures 8–15). These percentages also are plotted for all samples on a ternary sand-silt-clay diagram (Figure 16). (2) The data are plotted as cumulative curves to show grain-size distribution on logarithmic probability paper (Figure 17).

Ad 1.—The coarse-grained, sand-silt turbidites in rhythms 8–7 (Figure 9), 8A–18 (Figure 11), 10–5 (Figure 13), and 10–12 (Figure 14) exhibit distinct fining-upward grading. The grading is reflected by an upward decrease of sand-size material and an increase in silt- and clay-size particles.

Eriksson (1965), in an extremely detailed examination of core 210 of the Swedish Deep-Sea Expedition, located approximately 20 km to the west of core 10 of this study (Figure 1), found two types of sand-silt turbidites. One type, with a high percentage of bioclastic material, is distinctly graded. The second type, with a high percentage of terrigenous material, has less developed grading. However, this difference between the sand-silt tur-

Table 4.—*Percentages of sand-, silt-, and clay-size material in samples from eight rhythms analyzed (samples are identified by core number, rhythm number, and sample number, respectively)*

Sample no.	*Sand*	*Silt*	*Clay*	*Sample no.*	*Sand*	*Silt*	*Clay*
7–11–1	3	52	45	8A–18–9	1	42	57
2	1	46	53	10	12	33	55
3	5	43	52	11	13	30	57
4	6	42	52	9A–7–1	–	59	41
5	4	46	50	2	–	51	49
6	5	43	52	3	1	52	47
7	6	43	51	4	–	47	53
8	7	49	44	5	–	41	59
8–7–1	55	39	6	6	6	45	49
2	32	62	6	7	9	43	48
3	13	68	19	10–5–1	71	23	6
4	1	54	45	2	35	53	12
5	–	51	49	3	26	57	17
6	–	41	59	4	3	82	15
7	–	40	60	5	–	51	49
8	11	38	51	6	–	36	64
9	16	31	53	9	8	45	47
8A–11–1	2	76	22	10–12–1	69	18	13
2	–	55	45	2	39	51	10
3	–	38	62	3	25	52	23
4	–	34	66	4	9	77	14
5	1	47	52	5	–	41	59
8A–18–1	77	18	5	6	–	34	66
2	41	53	6	7	9	36	55
3	40	54	6	10A–19–1	1	63	36
4	4	89	7	2	–	46	54
5	2	75	23	3	–	43	57
6	–	69	31	4	6	43	51
7	–	46	54	5	11	44	45
8	–	38	62				

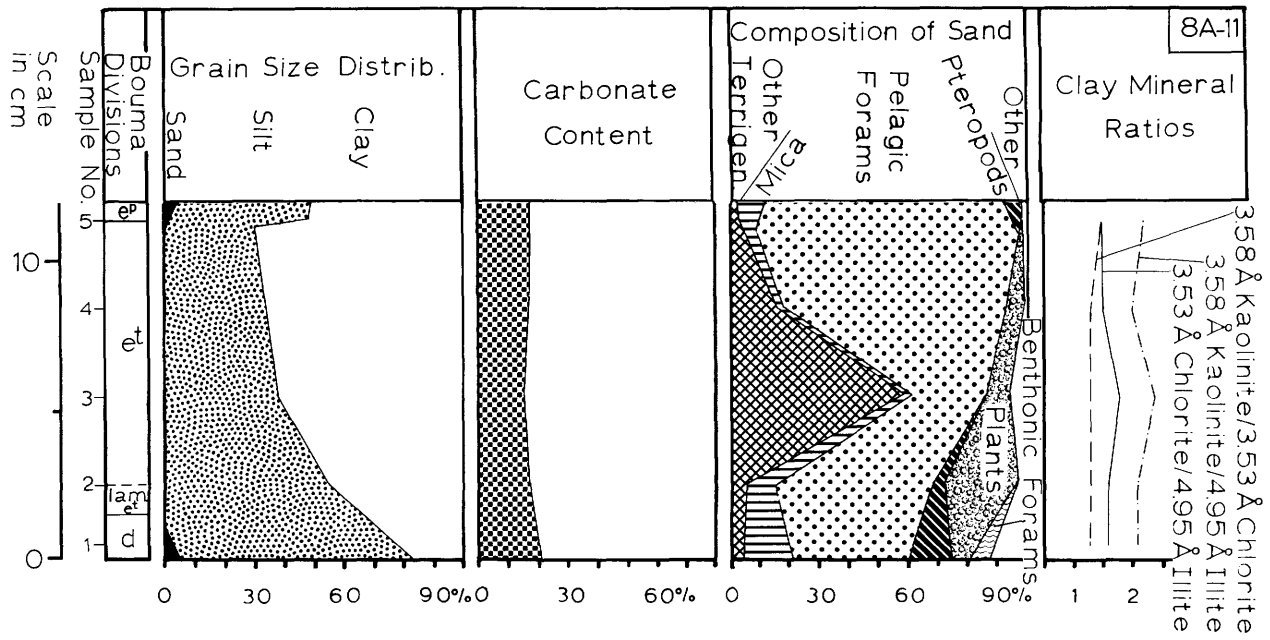

FIGURE 10.

bidites of largely terrigenous rhythms (8–7 and 8A–18) and largely bioclastic rhythms (10–5 and 10–12) is not observed.

Interestingly, the upper laminated division *d* shows a marked increase in the proportion of silt-size material. In the instance of rhythm 10–12, there is even a decrease in clay from the current ripple division *c* to division *d*.

Type A mud layers show a distinct fining-upward grading as well. The grading consists of an upward decrease of silt and an increase of clay. The shift in the silt-clay proportion can amount to as much as 20 percent. Most importantly, the grading of type A mud layers follows in regular fashion the grading of the underlying sand-silt turbidites or silt laminae. The sand-size fraction of type A mud is too low (less than 1 percent) to be plotted in the figures.

Type B mud layers exhibit no grading or, if anything, a slight coarsening-upward grading.

A distinct granulometric difference exists between type A and type B mud layers. The former contain, little, if any, sand, maximally 0.62 percent, with an average of 0.2 percent. The latter, however, contain a sizable amount of sand-grade material, maximally 16 percent, minimally 4 percent, with an average of 8 percent (Table 4; Figures 8–15). This sand is not graded as is that of the turbidite sand layers. In addition, type B mud layers show a lower amount of clay and, in some instances, an increase in silt content, as compared to the underlying uppermost part of type A mud layers.

The granulometric change across the boundary between type A and type B mud members can be sharp. Where the change is not abrupt, the boundary area is mottled and can show other signs of bioturbation.

The absence of a systematic, fining-upward grading in type B mud layers is shown and underscored by rhythm 7–11, in which type B mud is sampled over a thickness of 44.5 cm (Figure 8).

The grain-size characteristics of mud types A and B are difficult to compare with Eriksson's analysis of the fine-grained layers in core 210. Eriksson divides the fine-grained layers in several groups, based on the type of material present and particularly on what he interprets as wind-borne components. However, in the diagrammatic representation of his results, several rhythms as found in our cores can be recognized. Grading in mud layers following on top of sand-silt turbidites or silt laminae occurs. Also, on top of graded mud layers, muds with a higher sand percentage are

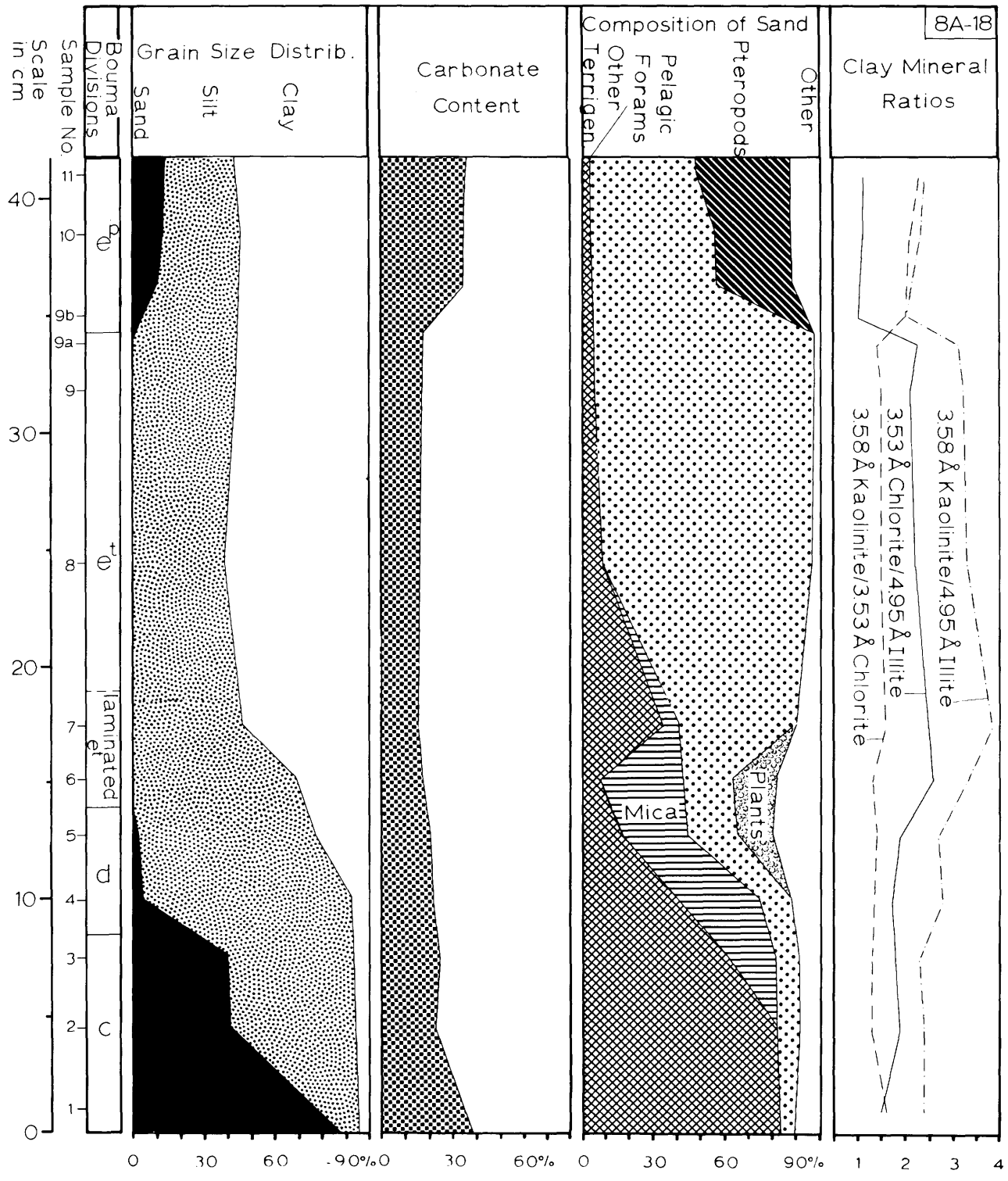
Scale in cm
Sample No.
Bouma Divisions
Grain Size Distrib.
Sand
Silt
Clay
Carbonate Content
Composition of Sand
Terrigen.
Other
Pelagic Forams
Pteropods
Other
8A-18
Clay Mineral Ratios
3.58 Å Kaolinite/4.95 Å Illite
3.53 Å Chlorite/4.95 Å Illite
3.58 Å Kaolinite/3.53 Å Chlorite
Mica
Plants
Laminated
0
30
60
90%
1
2
3
4

FIGURE 11.

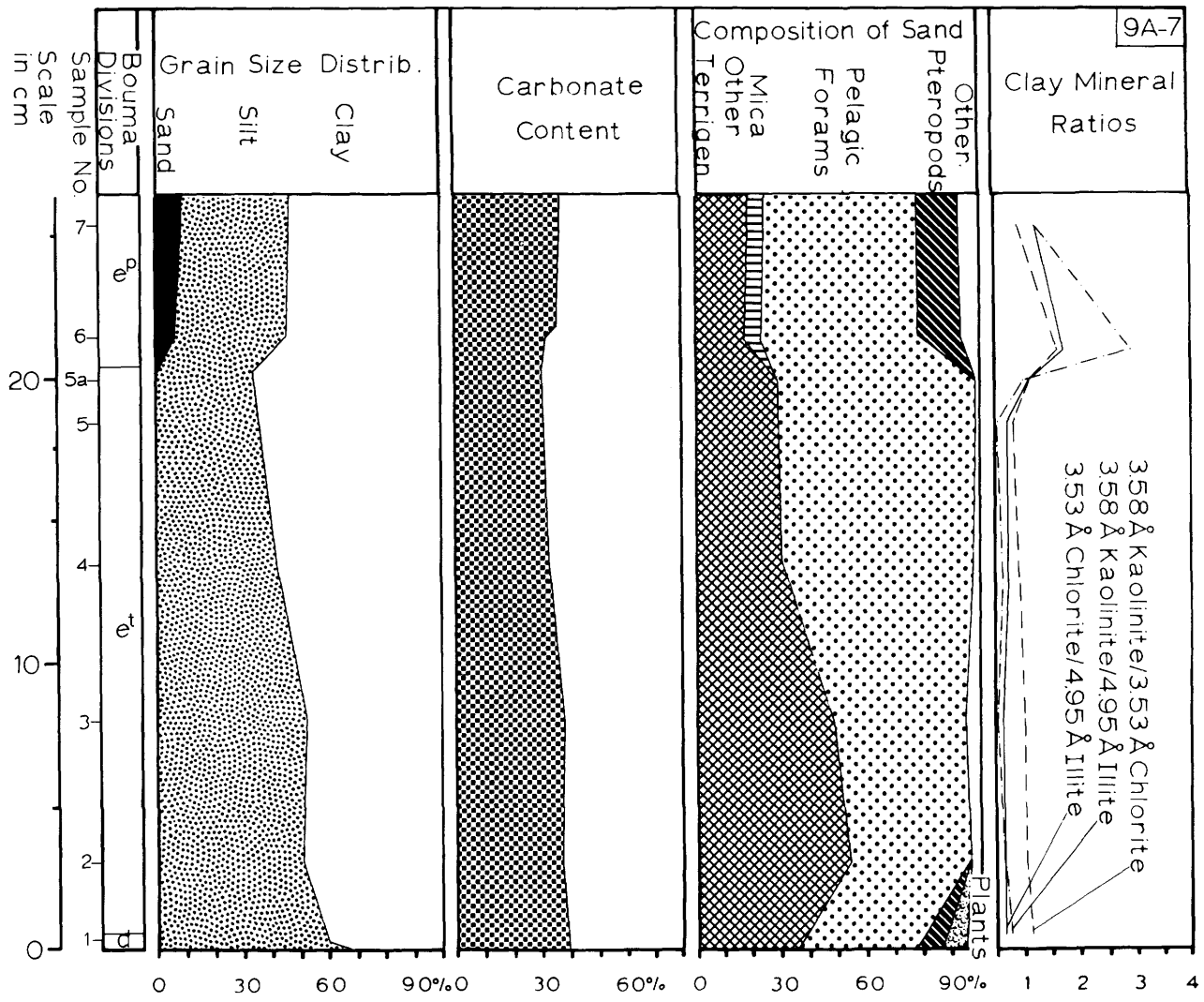

FIGURE 12.

indicated (cf., Eriksson, 1965, pl. 6, between depths of 484 and 443.5 cm in core 210).

The sand-silt-clay proportions of all 59 samples are plotted in a ternary diagram (Figure 16). A textural classification of the different rhythm members can be made, using the textural designations proposed by Folk (1961). The turbidite sand-silt layers, comprising the largest textural variety, include silt, sandy silt, silty sand, and, in one instance, muddy sand. The type A mud layers classify strictly as mud. The type B mud layers can be mud or sandy mud.

The diagram also shows differences in sorting between the three rhythm members. The turbidite sand-silt layers are the least sorted, whereas type A mud is the best sorted. Importantly, the diagram illustrates that the three rhythm members, defined primarily from X-radiographs, can also be recognized on the basis of textural analysis.

AD 2.—The cumulative grain-size curves (Figure 17) show even more distinctly the grading in the sand-silt turbidites. The lower, coarser grained part of the sand-silt layers exhibits coarse tail grading (the coarsest percentiles of the size distribution

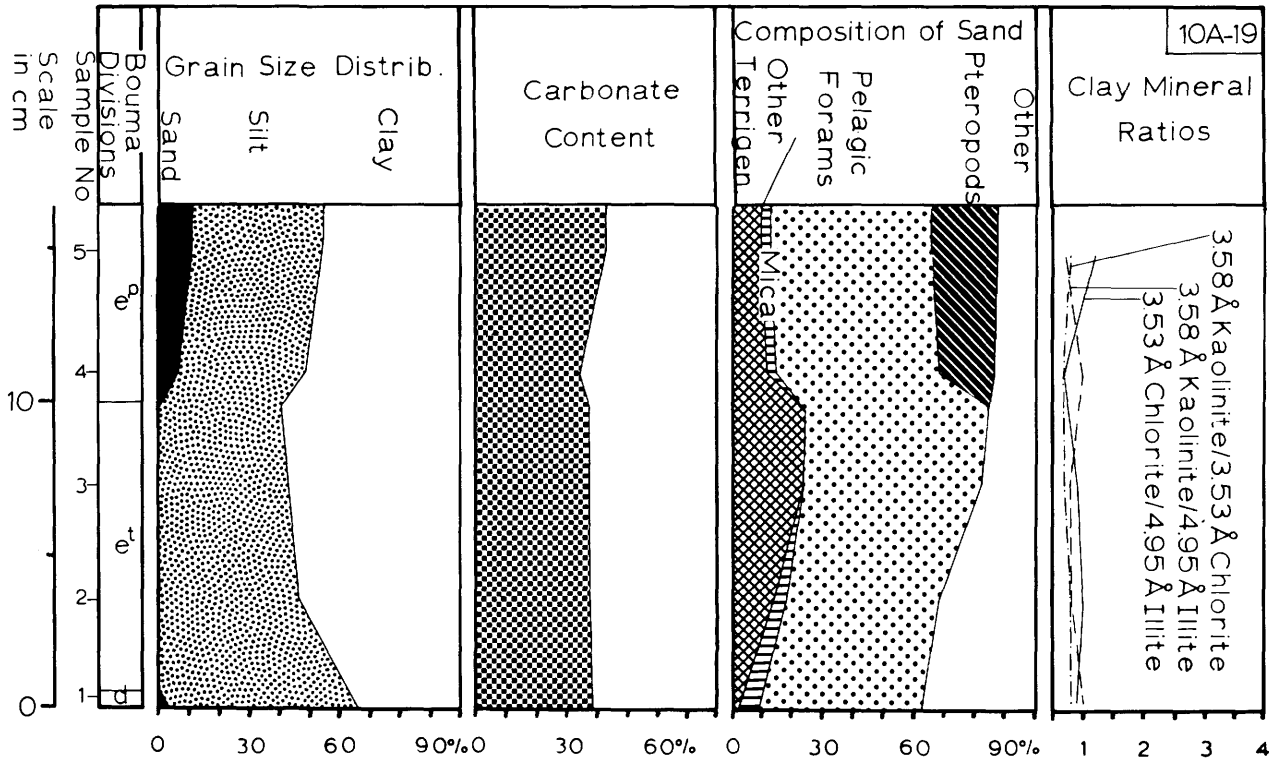

FIGURE 13.

show the grading, particularly well displayed in rhythm 8A–18). Type A mud layers are distribution graded (the entire size distribution shifts to finer sizes). Also shown clearly is that type B muds are not graded, neither internally, nor by a further size decline following that of the underlying type A mud.

Most importantly, the grain-size distribution within B type layers from various depths within the cores and from six cores at widely separated locations exhibits very little variation and is uniform. The uniformity within one B layer is particularly well shown for rhythm 7–11 (Figure 17). Type A mud layers, on the contrary, exhibit a much greater variability in grain-size distribution (Figure 17).

The average median diameter, as read off on the 50–percentile line, of type A muds (9.3 phi) is smaller than that of type B muds (9.1 phi), and it displays a larger spread (from 7.5 phi to 10.3 phi, as opposed to 8.4 phi to 9.5 phi).

The inclusive graphic standard deviation, or sorting, for type A mud is approximately 2, which is defined as poor to very poor (Folk and Ward 1957). The value for the sorting of type B mud is approximately 3, i.e., very poorly sorted. This difference in sorting can be clearly seen from the differences in slope of the cumulative curves (Figure 17).

The cumulative grain-size curves of type B mud tend to be straighter (almost perfectly so for some samples) than for type A muds. This means that the size distribution of the former approaches normalcy, more so than the latter.

Carbonate Content

The carbonate content of the eight rhythms was determined by gravimetric method, using the ascarite absorption technique. A small amount of sample (0.1 g) is treated with diluted HCl, and the liberated CO_2 is directed through vessels containing agents that remove possible other vapors to the ascarite tube. The carbonate percentage can be calculated from the weight increase of the ascarite tube. The accuracy of this method can be of the order of 1 percent. Results of the analyses are

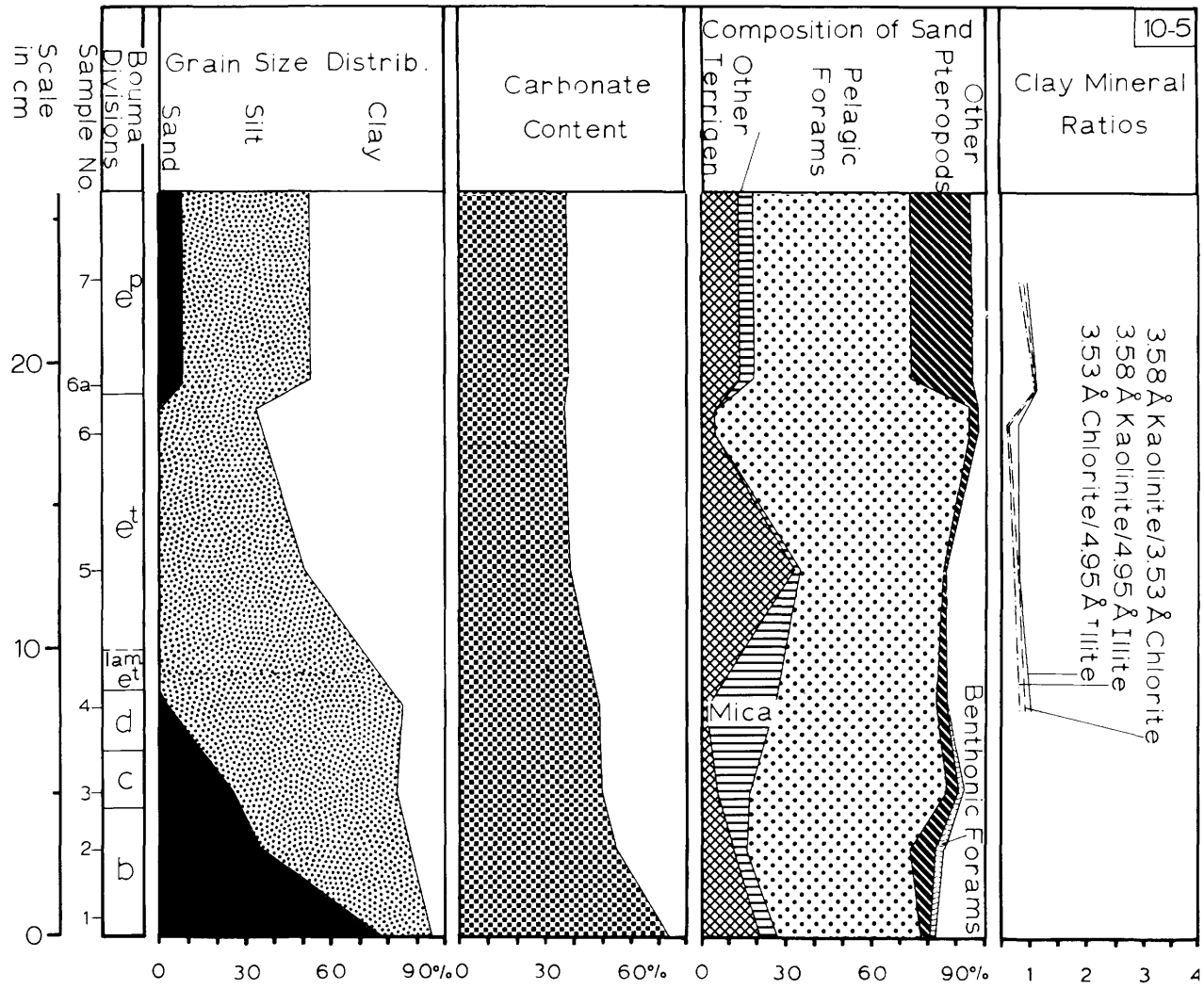

FIGURE 14.

detailed in Table 5 and depicted in Figures 8–15.

The turbidite sand-silt layers have the highest average carbonate content (40 percent) and the widest spread of values (from 21 to 74 percent). The overlying type A mud layers have the lowest average carbonate content (28 percent) and an intermediate spread (from 16 to 39 percent). The type B mud layers on top have an intermediate average carbonate content (35 percent) and the narrowest spread (from 26 to 46 percent).

In general, the carbonate content decreases with decreasing grain size. Within the sand-silt turbidites the carbonate percentage shows an upward decrease. In some of the type A mud layers, for example those of rhythm 9A–7 and 10–12, the carbonate content shows also an upward decrease by as much as 6 percent. As such, the A muds are not only texturally graded, but also compositionally. This compositional grading follows that of the underlying sand-silt turbidites.

The continuity from sand-silt turbidites to type A mud layers above them is illustrated by the fact that where the former are low in carbonate content the latter are proportionally low as well (8–7, 8A–18), and the reverse (10–5, 10–12). The carbonate content of the type B mud layers above

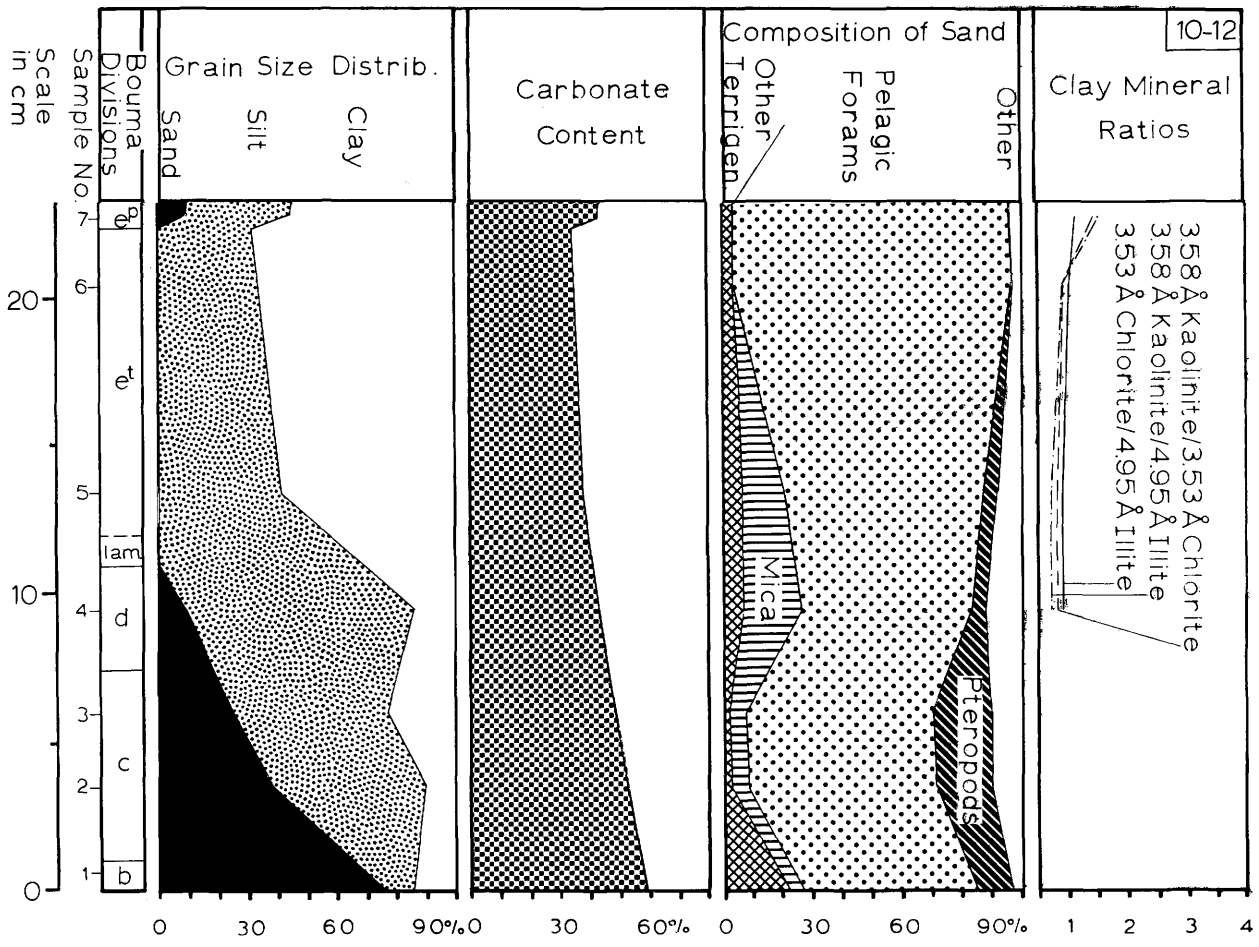

FIGURE 15.

these does not change and is independent of that of the underlying rhythm members.

The carbonate content of the type B layers is relatively constant. An abrupt change occurs across the boundary, where the underlying type A muds have a low carbonate content.

The carbonate materials are almost entirely biogenic in origin (see following section). Based on the carbonate content as an indication of the amount of biogenic components, the sand-silt turbidites fall into two classes, terrigenous (8–7, 8A–18) and biogenic (10–5, 10–12). The type A muds can be clayey muds (8–7, 8A–11, 8A–15) or marl muds (10–5, 10–12, 10A–19). The type A muds of rhythm 7–11 and 9A–7 are somewhat intermediate between terrigenous and biogenic types. Type B muds classify as marl oozes. Classification as used here follows that of the *Initial Reports of the Deep Sea Drilling Project* (Ryan, Hsü, et al., 1973c), and is modified after Olausson (1960).

Although only a few rhythms have been examined, it appears that the carbonate admixture of the sand-silt turbidites and the type A muds increases toward the west across the Balearic Abyssal Plain, i.e., from core 8 across the Balearic Abyssal Plain to core 10 and 10A.

Composition of the Sand Fraction

The larger than 63-micron fraction was obtained for all samples by wet sieving. Grain mounts were prepared for identification of the constituents and for determination of their relative frequencies. Relative frequencies were determined by counting

300 to 400 grains per mount. Due to the very small percentage of sand-grade material in the samples from type A mud layers, no technique of point counting could be practiced. Instead, all grains per unit area were counted. As a result, bioclastic particles of large size (e.g., pteropod shells of low effective density) are relatively underrepresented as compared to smaller particles (e.g., quartz grains of high effective density).

Constituents were counted and grouped in the following classes: terrigenous (mica and other, including quartz), bioclastic remains (pelagic forams, benthonic forams, pteropods, and other), plant fragments, and other (including ostracode valves, sponge spicules, unidentifiable fragments, etc.). The results are given in Table 6 and Figures 8–15, 18, and 19.

TABLE 5.—*Carbonate percentages for samples from eight rhythms studied (samples are identified by core number, rhythm number, and sample number, respectively)*

Sample no.	$CaCO_3$ %	*Sample no.*	$CaCO_3$ %
7-11-1	28	8A-18-9	18
2	25	10	35
3	28	11	36
4	28	9A-7-1	39
5	26	2	37
6	28	3	38
7	28	4	33
8	29	5	32
8-7-1	33	6	32
2	24	7	37
3	25	10-5-1	74
4	21	2	55
5	22	3	50
6	21	4	49
7	22	5	39
8	40	6	37
9	46	7	38
8A-11-1	25	10-12-1	60
2	22	2	–
3	20	3	–
4	22	4	43
5	22	5	38
8A-18-1	38	6	35
2	23	7	43
3	25	10A-19-1	39
4	22	2	38
5	21	3	38
6	18	4	35
7	16	5	43
8	17		

The widest variety of constituents occurs in the turbidite sand-silt layers. The terrigenous components are mainly quartz, mica, and feldspars. A wide spectrum of foram tests, both pelagic and benthonic, is represented by their microskeletal remains. Other organic remains include those of pteropods, crinoids, ostracods, sponges, and plants. A few siliceous remains from radiolarians and diatoms also occur. Glauconite is present as well.

This association of microfossil and other organic remains is typical for resedimented deposits containing biogenic remains from various environments (terrestrial, neritic benthonic, bathyal or abyssal benthonic, and pelagic) (Parker, 1958). The constituents are very poorly sorted, and the shelly remains commonly are broken (Figure 18A,C).

The constituents of type A mud layers are largely the same as those of the underlying sand-silt turbidites; the individual specimens of each constituent, however, are markedly smaller on the average in the type A mud layers. In the top part of these layers, large *Orbulina* specimens can be found. Their sizes are quite uniform (well sorted), and the foram tests are only slightly larger than the quartz grains.

Fecal pellets and remnants of pyritized burrow tubes occur in type A layers as well, particularly near the boundary with the overlying type B layers.

Type B layers can contain quartz, mica, and feldspar, though in small proportions. The organic remains show less variety. Skeletons of pelagic forams and pteropods form the main constituents. Among the rest are sponge spicules, radiolarian, diatomaceous, and crinoid fragments. The spread of particle sizes is wide (very poor sorting) (Figure 18B,D).

The quartz grains in the three types of layers often are of the so-called desert type, i.e., rounded and stained, or frosted (Eriksson 1965).

In the turbidite sand-silt layers, concentrations of different constituents are associated with specific sedimentary structures (Figures 8–15). For example, the mica flakes and plant fragments occur most frequently in the *d*-division. This indicates that the relative frequencies of the components are determined to a large degree by their hydrodynamic properties. Vertical sorting appears to have taken place according to the effective densities of the components. Light, large, nonspherically (oblately) shaped particles are therefore concentrated in the

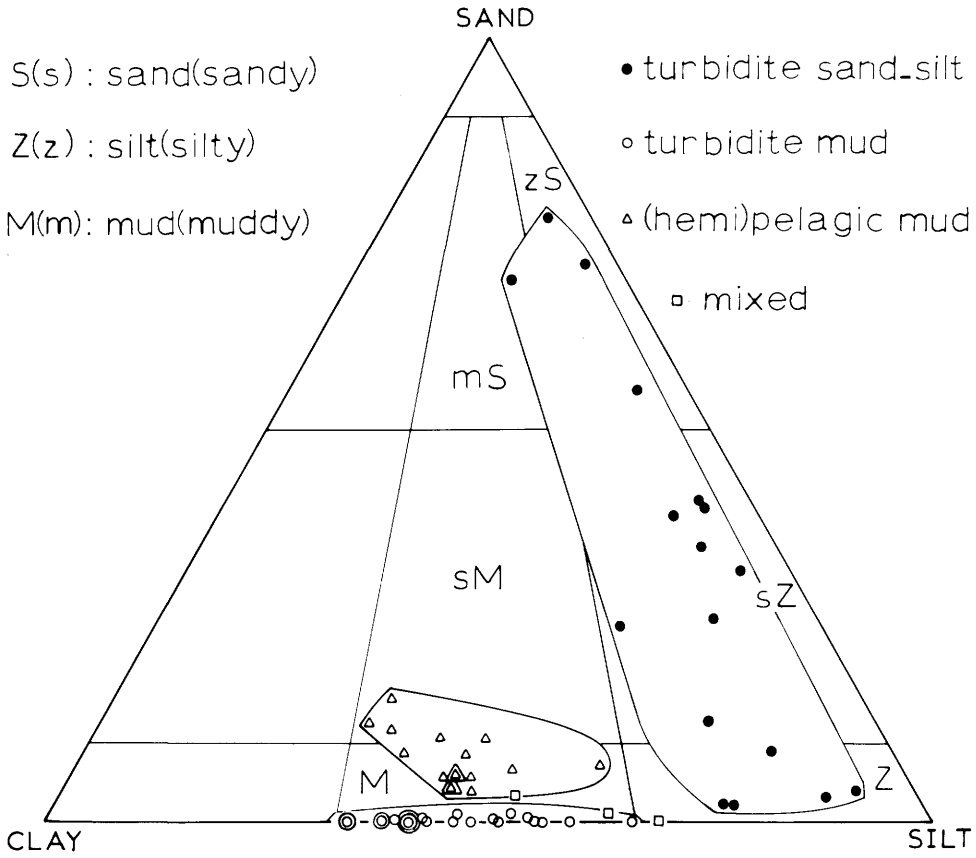

FIGURE 16.—Ternary diagram in which are plotted the sand-silt-clay proportions of all samples of eight studied rhythms. Different symbols show turbidite sand-silt layers, type A mud layers (interpreted as turbiditic), and type B mud layers (interpreted as hemipelagic). The mixed samples are from boundary regions between two rhythm members.

d-division, while smaller, but spherical, particles of higher effective densities occur in the lower structural divisions.

This phenomenon of vertical sorting of different components according to their hydrodynamic properties continues without a break from the turbidite silt layers into the type A mud layers. Mica flakes and plant fragments remain relatively frequent in the lower part of type A muds. In the upper half of these layers, tests of pelagic forams occur in high relative frequency. The forams exhibit a small size range (well sorted) (Figure 18E), and the size of the few associated quartz grains is consistently somewhat smaller.

An abrupt change in relative proportions occurs across the boundary into type B muds (Figure 19). The constituents are mainly remains of pelagic forams and pteropods (Figure 18B,D). Mica and a few other terrigenous particles are present as well. The mica content increases somewhat, as do the pteropod shells. Pelagic foram tests, on the other hand, decrease relatively. Plant fragments are virtually absent (Figure 19). Within the type B mud layers no systematic change in proportions or constituents occurs, and apparently no hydrodynamic sorting effective on the sea floor has influenced their sand composition. The components are of widely varying sizes (very poorly sorted) (Figure 18B,D).

The composition of sand-grade material in terrigenous sand-silt turbidites and type A mud layers differs from sands in bioclastic layers in that the former have significant proportions of plant remains and a higher proportion of terrigenous

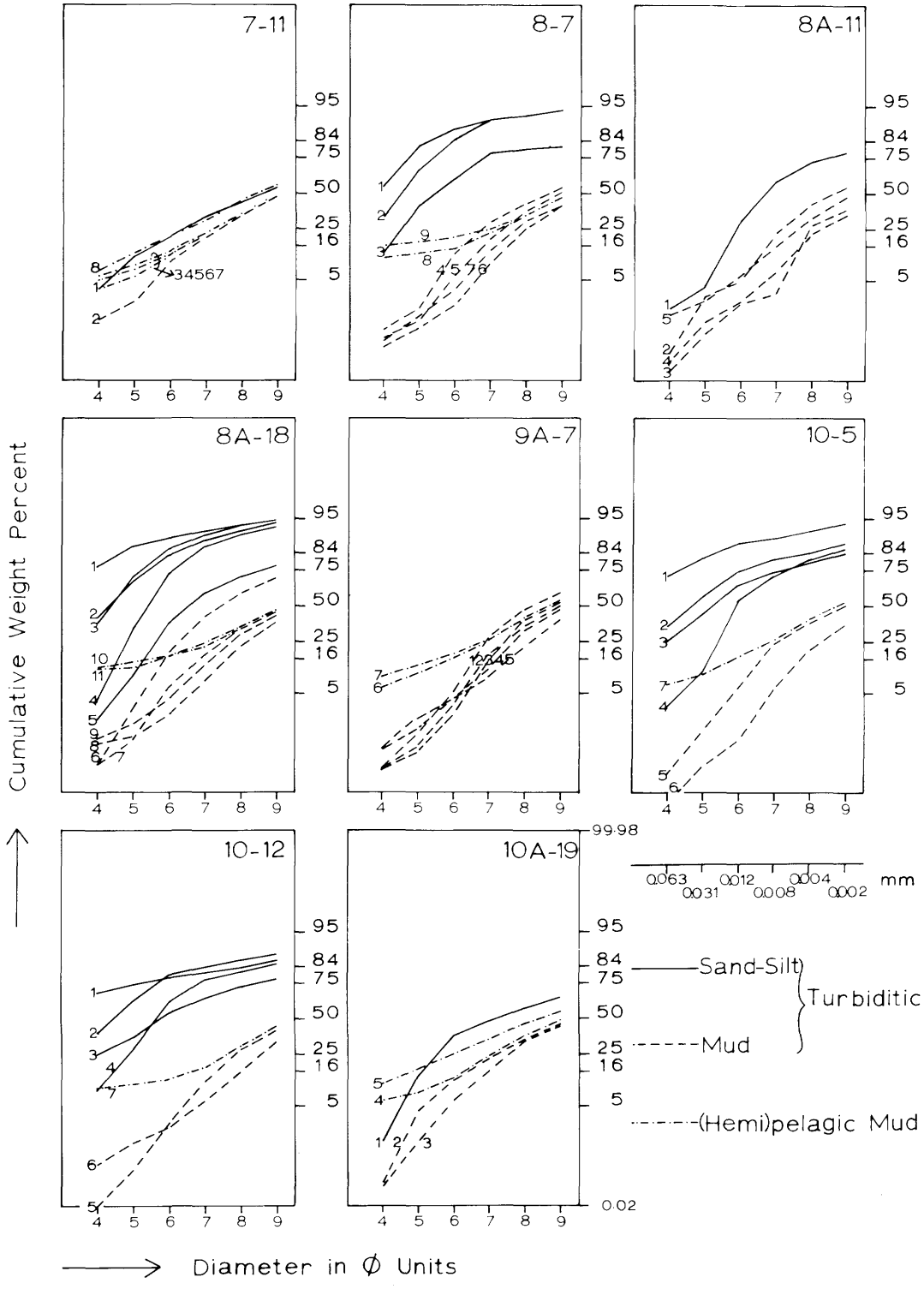

FIGURE 17.—Cumulative grain-size curves for all samples from the eight studied rhythms. Different lines are used for samples from turbidite sand-silt layers, type A mud layers (interpreted as turbiditic), and type B muds (interpreted as hemipelagic). Sample numbers are indicated on the curves.

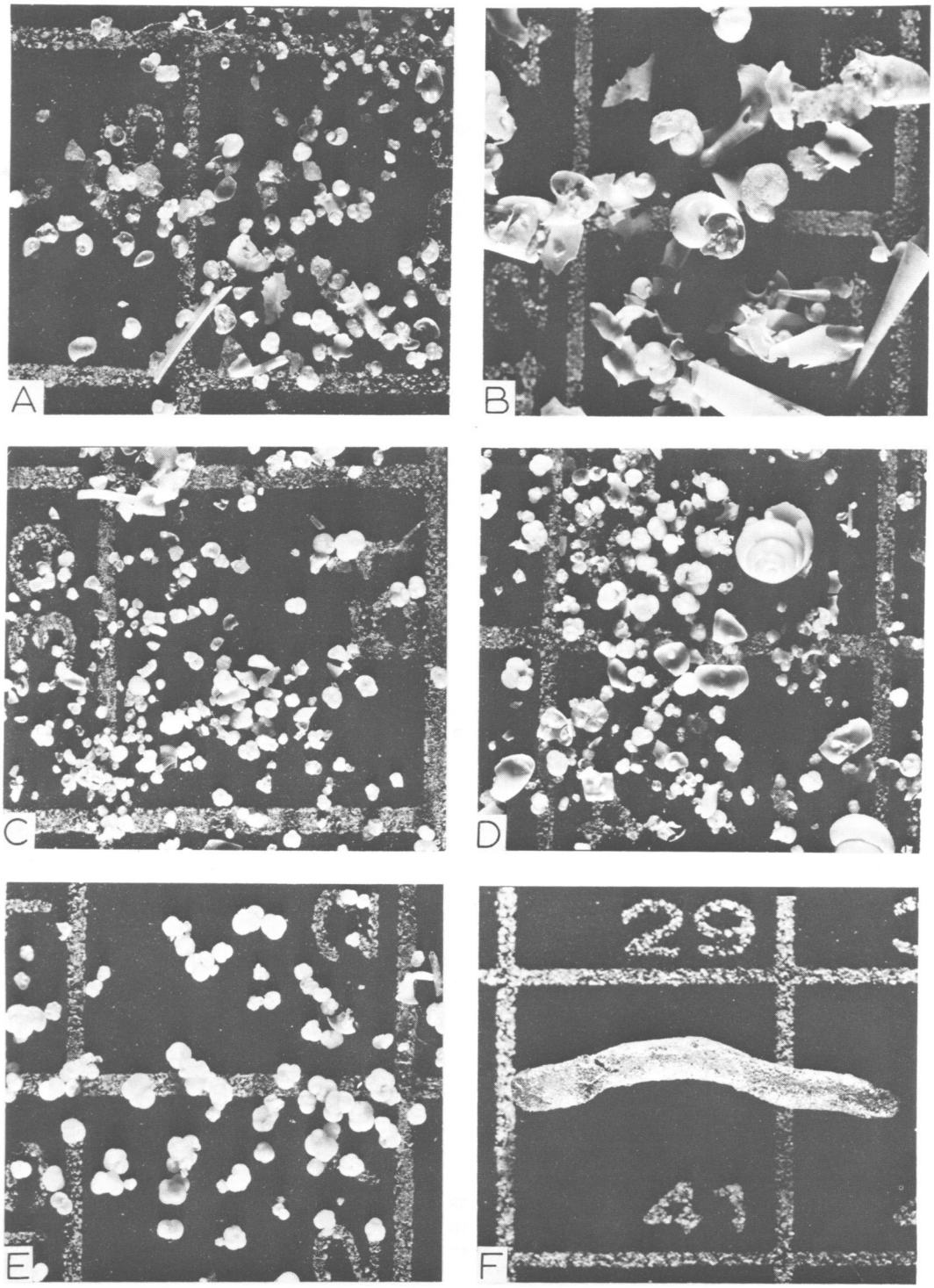

FIGURE 18.—Photomicrographs of the coarser than 63 micron fraction of turbidite sand layers (A, C), and type B mud layers (B, D). The corresponding sample numbers from A to D are: 8–7–1, 8–7–9, 10–5–1, and 10–5–7. E = forams in sample 10–5–6. F = pyritized filament in sample 9A–7–4. The white lines (on background) form squares that measure 3.7 by 3.7 mm.

TABLE 6.—*Percentages of the different components, comprising the sand-size fraction of eight rhythms studied (samples are identified by core number, rhythm number, and sample number, respectively)*

Sample no.	Terrigenous		Pelagic	Benthonic			
	Mica	Other	forams	forams	Pteropods	Plants	Other
7-11-1	8	25	43	3	1	–	20
2	12	23	50	2	1	–	12
3	7	25	29	1	27	–	11
4	8	13	37	1	34	–	7
5	4	8	48	1	33	–	6
6	5	11	54	1	24	–	5
7	5	13	43	1	28	–	10
8	9	24	48	–	15	–	4
8-7-1	80	5	11	–	3	–	1
2	73	6	13	–	3	–	5
3	45	15	21	–	6	12	1
4	6	44	17	–	–	30	3
5	30	24	16	–	–	29	1
6	71	4	14	–	1	5	5
7	7	–	89	–	1	1	2
8	–	–	35	2	55	–	8
9	1	–	38	2	54	–	5
8A-11-1	16	4	41	7	13	8	11
2	10	5	53	1	3	26	2
3	3	61	25	–	–	7	4
4	3	15	74	–	–	7	1
5	8	2	84	–	4	1	1
8A-18-1	–	83	6	1	2	–	8
2	–	82	9	–	2	–	7
3	16	65	10	–	2	–	7
4	33	41	14	–	2	–	10
5	31	13	21	–	2	15	18
8A-18-6	36	6	21	–	–	19	18
7	6	34	50	–	–	–	10
8	–	8	89	–	–	–	3
9	–	5	93	–	–	–	2
10	–	3	53	1	32	–	11
11	–	3	45	1	40	–	11
9A-7-1	30	7	42	1	5	8	7
2	10	43	43	1	2	–	1
3	–	48	47	–	–	–	5
4	–	30	68	–	–	–	2
5	–	29	70	–	–	–	1
6	*	22	54	–	18	–	6
7	–	24	51	–	19	–	6
10-5-1	5	18	53	2	4	–	18
2	4	11	58	3	9	–	15
3	11	5	70	2	4	–	8
4	24	1	57	–	4	–	14
5	2	32	51	1	1	–	13
6	–	4	90	–	3	–	3
7	5	13	55	1	22	–	4
10-12-1	4	19	60	–	13	–	4
2	6	2	63	2	19	–	8
3	6	1	62	3	20	–	8

TABLE 6.—Continued

Sample no.	Terrigenous		Pelagic	Benthonic			
	Mica	*Other*	*forams*	*forams*	*Pteropods*	*Plants*	*Other*
4	20	6	57	1	5	–	11
5	14	6	67	1	6	–	6
6	–	3	94	–	–	–	3
7	–	3	93	–	–	–	4
10A–19–1	8	1	54	1	1	–	35
2	4	13	51	1	1	–	30
3	1	22	59	1	1	–	16
4	4	10	54	1	20	–	11
5	3	9	53	–	22	–	13

constituents such as quartz and mica. The virtual absence of plant remains in bioclastic turbidites in the Caribbean has been reported by Rusnak and Nesteroff (1964).

Figure 19 summarizes the average relative frequencies of the sand constituents as distributed through the eight terrigenous and bioclastic rhythms examined in this study. The boundary between the lower coarse-grained member and type A mud is markedly different from the one between mud types A and B. Across the former boundary, a continuity of components and their gradually changing proportions is noted. Across the latter an abrupt change occurs, most clearly indicated by a small increase in mica, a decrease in pelagic foram tests, and an increase in pteropod shells. It should be emphasized that these changes as schematically depicted are changes in relative frequencies, not necessarily in absolute numbers. For example, the relative frequency of pelagic foram tests is shown to decrease, although the absolute number, in fact, increases due to the much higher percentage of sand (indicated in the second column of Figure 19). In contrast, Weidmann (1967) in a similar diagram schematically illustrates a relative increase in pelagic foram tests in the top layer.

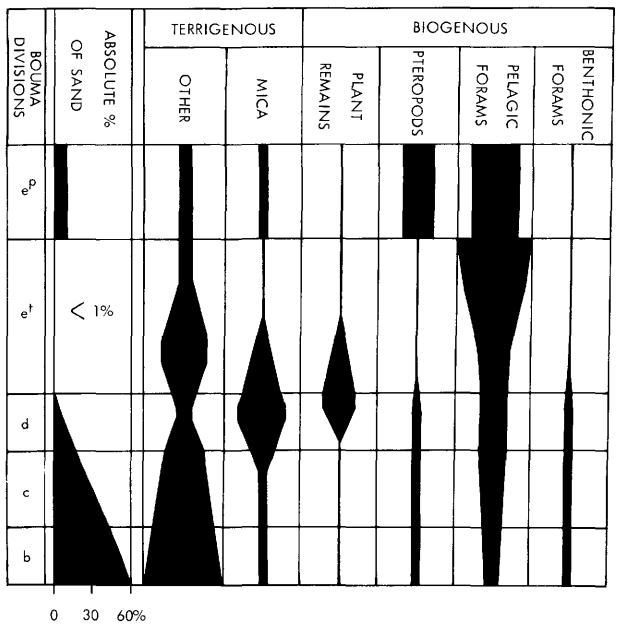

FIGURE 19.—Summary diagram showing the relative frequencies of the major constituents in the sand-size fraction of the eight rhythms studied. The columns for mica and plant fragments are typical for terrigenous turbidites and type A muds (interpreted as turbiditic, or e^t).

An absolute increase in the number of foram and pteropod remains in the top part of fine-grained layers following turbidite sand-silt layers has also been described by Nesteroff (1961), Nesteroff and Heezen (1963), and Rusnak and Nesteroff (1964).

CLAY MINERALOGY

The samples were mineralogically analyzed by X-ray diffractometry. The instrument used was a Noralco (Philips) unit, with Cu K-alpha radiation and Ni filter. Slides were prepared from grain-size fractions separated by the pipette method. Both the finer than 4 phi and the finer than 9 phi fractions were used. Some slides were glycolated (overnight in glycol vapor).

The minerals present are: quartz, calcite, dolomite, kaolinite, chlorite, illite, plagioclase, K-

feldspar, and montmorillonite (not always in this order of relative abundance). The latter mineral forms no distinct peak. In the finer than 9 phi fraction the dolomite is absent and feldspars in most instances are not observed. These minerals are present in all rhythms but in varying proportions.

The major clay minerals are illite, chlorite, and kaolinite; montmorillonite, detected by glycolation, is present in minor quantities. This confirms earlier studies of clay mineralogy in the western Mediterranean by Nesteroff, Sabatier, and Heezen (1965).

A study of the relative abundances of the three clay minerals was made by an analysis of peak heights. The peaks used are for illite: d–4.95, for chlorite: d–3.53, and for kaolinite: d–3.58. All samples exhibit these peaks quite distinctly, and the kaolinite and chlorite peaks can be easily distinguished with a rotation of one-half degree (2 theta) per minute (Figure 20). The results are listed in Table 7.

TABLE 7.—*Peak-height ratios of C (chlorite, d–3.53 Å), I (illite, d–4.95 Å), and K (kaolinite, d–3.58 Å), for samples from eight rhythms analyzed (samples are identified by core number, rhythm number, and sample number, respectively)*

Sample no.	*C/I*	*K/I*	*K/C*	*Sample no.*	*C/I*	*K/I*	*K/C*
7–11–1	1.0	2.5	2.6	8A–18–8	2.2	3.3	1.5
2	1.1	3.3	3.0	9	2.1	3.2	1.5
3	1.1	2.3	2.1	9a	2.3	3.1	1.4
4	1.1	2.3	2.1	9b	1.0	2.0	2.0
5	0.8	2.4	2.9	10	1.1	2.3	2.1
6	1.3	3.1	2.5	11	1.1	2.4	2.3
7	0.9	2.4	2.6	9A–1–1	0.6	0.7	1.1
8	1.0	1.8	1.8	2	0.6	0.6	1.0
8–7–1	2.0	2.7	1.4	3	0.6	0.5	1.0
2	2.2	2.7	1.2	4	0.7	0.6	0.9
3	1.4	2.1	1.5	5	0.7	0.5	0.8
4	2.2	2.6	1.1	5a	1.1	1.1	1.1
5	1.8	2.2	1.3	6	1.7	2.9	1.6
6	1.4	1.8	1.3	7	1.2	1.2	0.9
7	1.4	2.5	1.7	10–5–4	1.0	0.8	0.9
8	1.6	1.6	1.0	5	0.8	0.7	0.8
9	1.4	2.1	1.5	6	0.8	0.6	0.8
8A–11–1	1.6	2.1	1.3	6a	1.1	1.1	1.1
2	1.6	2.1	1.3	7	0.9	0.8	0.9
3	1.8	2.4	1.3	10–12–4	0.9	0.7	0.8
4	1.5	2.0	1.3	5	0.9	0.7	0.8
5	1.5	2.2	1.5	6	1.0	0.9	0.9
8A–18–1	1.5	2.4	1.6	7	1.1	1.5	1.4
2	1.9	2.4	1.3	10A–19–1	0.9	0.8	1.0
3	1.8	2.3	1.3	2	1.0	0.8	0.8
4	1.7	2.8	1.7	3	0.9	0.7	0.8
5	1.9	2.7	1.4	4	0.7	0.7	1.0
6	2.6	3.3	1.3	5	1.2	0.8	0.7
7	2.5	3.9	1.6				

The peak-height ratios have been plotted against the sample points for each rhythm (Figures 8–15). The ratios are, in most instances, different for the type A and type B muds of a particular rhythm. A sharp break in the curves of the clay-mineral ratios can occur at the boundary between the two kinds of mud. This mineralogical change is particularly noticeable in rhythms 8A–18 and 9A–7. Extra samples were taken as near to the boundary as possible to verify the abruptness of the change (samples marked by a or b). The change in illite, kaolinite, and chlorite peaks between the two samples on either side of the boundary of rhythm 9A–7 is illustrated in Figure 20.

The change of clay ratios from type A into type B muds is most pronounced where the A muds are terrigenous (8–7, 8A–18, 9A–7) and less so where they are bioclastic (10–5, 10–12, 10A–19). The clay-mineral suites of terrigenous A mud, bioclastic A mud, and of type B mud show each a rough uniformity. The proportion of clay minerals is different in each mud type.

Discussion

Types of Depositional Mechanisms

There is evidence for several depositional mechanisms operating in the abyssal environment of the western Mediterranean:

1. Normal, pelagic settling of terrigenous particles introduced by rivers and wind, and of marine microskeletons. Fine-grained sediment layers in cores from the Algéro-Balearic Basin have been attributed to this process (Eriksson, 1965; Leclaire, 1972a, 1972b).

2. Turbidity currents transporting dominantly terrigenous materials from shallower environments onto the abyssal plain. Coarse-grained turbidites have been identified in a number of cores from the Balearic Abyssal Plain (Horn, Ewing, and Ewing, 1972).

3. Normal bottom currents of various types, eroding, transporting, and redistributing sediments on the sea floor. The lower section of the Balearic Basin fill, as recovered at JOIDES drilling site 124,

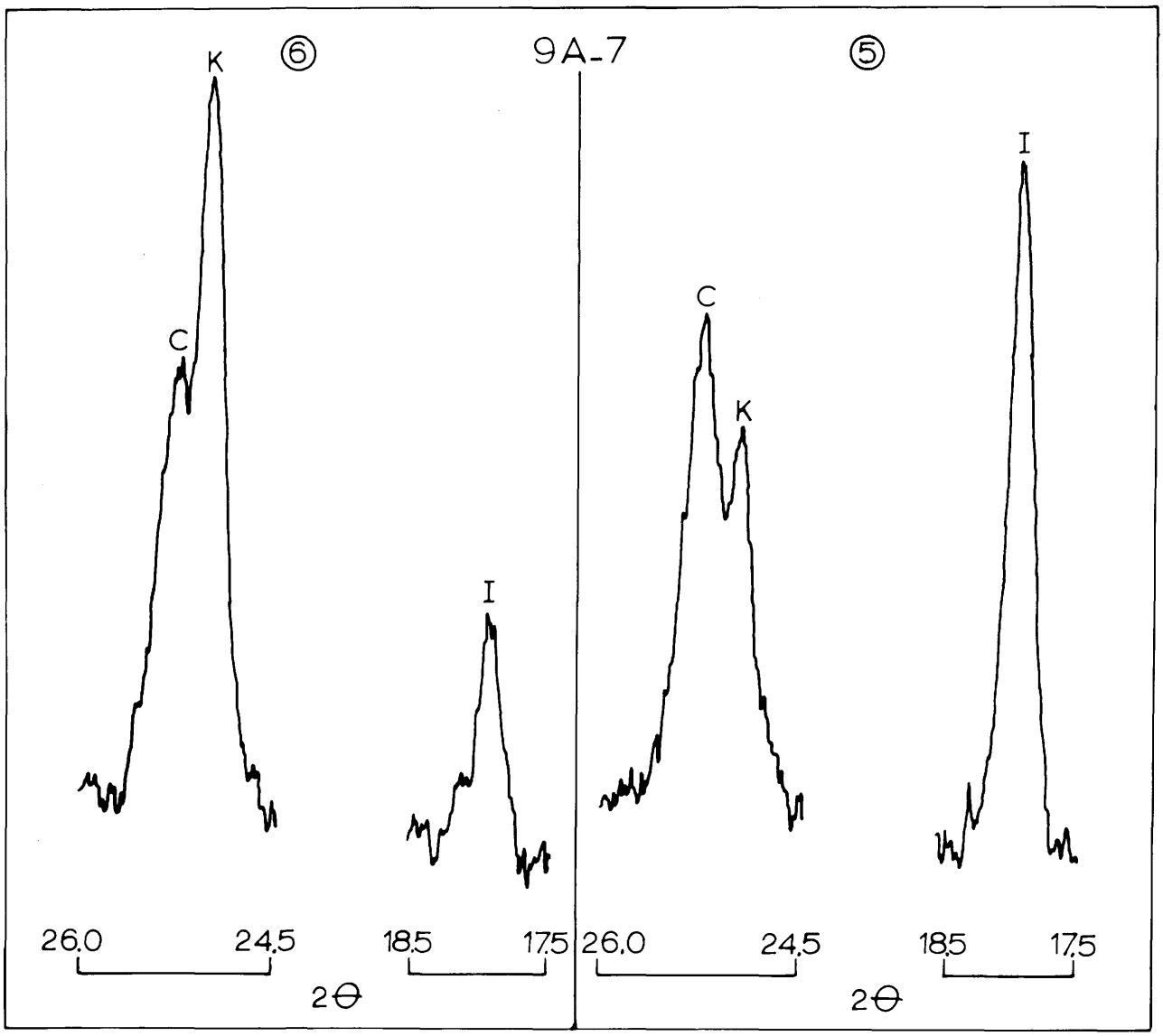

FIGURE 20.—Peaks from X-ray diffractograms of 4.95 A illite (I), 3.58 A kaolinite (K), and 3.53 Å chlorite, illustrating sharpness of peaks and change in peak-height ratios from sample 9A–7–5 (type A mud) to 9A–7–6 (type B mud).

is attributed to the redepositing activity of contour-type currents (Nesteroff, 1973). Strong bottom water movement is noted in shallow straits at the basin margin (Strait of Sicily and Gibraltar region; Lacombe, 1971; Kelling and Stanley, 1972a,b). On the other hand there is little direct evidence available in support of well-defined bottom currents, although physical oceanographic data suggest the westerly movement of potentially active but transient bottom currents in the region off North Africa and the Balearic-southeastern Iberian platform (Miller, 1972).

4. Certain types of low density, gravity-assisted currents transporting largely terrigenous clay-size particles down the continental slope-rise. Muds in the Alboran Sea are attributed to this mechanism (Bartolini and Gehin, 1970; Stanley, Gehin, and Bartolini, 1970; Huang and Stanley, 1972).

Mud Deposition—General

Nesteroff (1961; also Nesteroff and Heezen, 1963; and Rusnak and Nesteroff, 1964) describes the typical sequence of structures in oceanic turbidites, and the distribution of foram and pteropod skeletons in these. His typical sequence ("séquence type") is quite similar to the type 1 rhythm of this study: a sand-silt layer is followed by a mud layer containing very little sand-grade material, which in turn is followed by a layer of mud with a high concentration of foram test and pteropod shell material. The explanation offered is that the entire sequence formed by a turbidity current, the tail of which carried skeletal material of extremely low effective densities that became incorporated in the upper part of the deposit. Pelagic sediments are thought to have been eroded by turbidity currents. Kuenen (1964) interprets the upper layer of shell material as winnowed concentrates from a pelagic stratum by the turbidity current that deposited the covering turbidite, though in some instances it may represent the pelagic stratum.

From the foregoing analysis, however, it appears that type A and B mud layers formed from different depositional mechanisms. The break in texture and composition across the boundary between them excludes the explanation of continuous deposition from a turbidity current for both mud layers combined. Also the relatively high clay content and the poor sorting of the B muds exclude winnowing bottom currents as a mechanism.

Turbiditic Mud Deposition—Type A Muds

The assemblage of characteristics of the type A mud layers can be best explained by deposition from turbidity currents. The following features support this interpretation.

Structural.—On X-radiographs the lower portion of several type A mud layers exhibits delicate lamination (8A–11, 8A–18, 10–5, 10–12). As such, a structural continuity exists from the upper laminated *d*-division into type A mud layers (Figure 4).

Normal pelagic settling does not produce lamination due to the continuous organogenic disturbance of the slowly accumulating particles. Laminations can form in stagnant water of which the lower portion has become anaerobic (van Straaten, 1967). The presence of benthonic life, however, is evident from burrow tubes. Bottom photographs also show that the modern plain surface is affected by the activity of animals (Heezen and Hollister, 1971).

Textural.—Type A mud layers show distribution grading following the coarse tail grading of the lower part of the sand-silt turbidites where these are present. Experiments indicate that coarse tail grading is produced by high density turbidity currents, whereas distribution grading results from relatively dilute flows (Middleton, 1967). Also, the sorting of type A muds is better developed than that of type B mud layers, which can be interpreted as the effect of hydrodynamic selection during current transportation. The fact that type A muds are poorly sorted nevertheless excludes normal bottom currents as depositional mechanism. Contourites, for example, exhibit good to very good sorting (Bouma, 1972a, 1972b).

Compositional.—The carbonate content of some type A mud layers shows an upward decrease and, as such, a compositional grading which follows that of the underlying sand-silt turbidites where present. The overall carbonate content of type A muds varies with that of the underlying turbidite sand-silt layers.

Such compositional grading as indicated by the carbonate content is documented as well for very thick turbidite marlstone layers following on top of very thick turbidite calcarenites in the Eocene flysch of the southwestern Pyrenees (Rupke, 1972).

The individual components of the sand-grade fraction, in particular the mica and the plant particles, are concentrated in the upper *d*-division of the turbidite sand-silt layers and in the lower portion of the type A muds. This continuity of composition cannot be attributed to biogenic homogenization of the boundary area, otherwise the delicate lamination would have been obliterated.

In general, structural, textural, and compositional continuity from the sand-silt turbidites into the type A mud layers suggests that they formed from a single turbidity current. The genetic connection between coarse-grained turbidites and their overlying type A muds excludes permanent or semipermanent low-density suspension currents as the depositional mechanism of the type A muds, and indicates emplacement by the tail of a normal, high-density turbidity current (Kuenen, 1967). In short, type A muds are the turbiditic portion of the

pelitic *e*-division, symbolized as e^1 (Figures 8–15).

Where only thin silt laminae or lamels form the beginning of a rhythm, the type A mud layers are likely to be the distal portion of a turbidite body, deposited by the slowly moving, or ponded, less dense tail of a normal, high-density turbidity current. Such layers can be designated as mud turbidites. However, the depositional mechanism for mud turbidites can also be an originally low-density turbidity current, triggered, for example, by stirred up fine sediment on the shelf-break during storms (Stanley, 1969, 1970).

Further evidence for deposition by gravity-propelled density currents of type A muds, rather than by normal pelagic settling, comes from the fact that the proportion of type A mud, as well as that of turbidite sand-silt, is higher in the cores from greater water depth (Figure 6). This is to be expected where turbidity currents seek the lowest parts of the basin plain. In contrast, the proportions of type B muds show an inverse relationship with the water depth of the cores.

Hemipelagic[3] Mud Deposition—Type B Muds

The properties of type B mud layers fit best the depositional process of pelagic settling. Evidence for this comes from the following observations.

Structural.—All type B mud layers lack any kind of primary sedimentary structure, including fine lamination. Pelagic deepwater deposits do not become laminated due to the fact that the slowly accumulating particles are constantly being rearranged by benthonic organisms. Accordingly, burrowing structures are present in type B muds.

Textural.—Type B muds exhibit no systematic changes in grain-size distribution. In addition, the grain-size distribution of all type B layers is virtually uniform throughout the basin area examined and is constant through time as well. This uniformity of type B mud layers is a typical feature of pelagic deposition and cannot be explained by other depositional processes.

The high clay content and very poor sorting of the type B muds excludes any normal bottom current emplacement.

Compositional.—The composition of the type B muds is typical of autochthonous deepwater accumulations. The components of the coarser fraction are mainly from pelagic organisms, dominantly forams and pteropods. The shelly remains are largely unbroken and unworn, even the delicate pteropod skeletons. In addition, the composition of type B layers varies little from one to the other, unlike type A muds.

The interpretation of type B muds as hemipelagic deposits is significantly strengthened by an analysis of radiocarbon dates determined on their carbonate sands. In summary, type B muds constitute the hemipelagic upper part of the pelitic *e*-division, or the e^1 (Figures 8–15).

Normal Bottom Current Activity

In addition to evidence for turbidity currents and pelagic settling, evidence for occasional bottom current activity exists. Within type B mud layers, concentrations of coarse skeletal remains can occur with a low pelite content (for example two of these accumulations are observed in Figure 4:8–20). Van Straaten (1967) found pteropod shell layers in the Adriatic on top of ash layers and interpreted their origin to mass death caused by a natural clamity such as a volcanic eruption. No ash occurs in the type B mud layers in question, and the most logical explanation would seem to be a winnowed concentrate formed by normal bottom currents. It is also possible, however, that such skeletal remains accumulate as a result of periods of particularly high productivity (Huang, Stanley, and Stuckenrath, 1972). Such shell concentrates only occur in type B layers, never in type A muds. This is to be expected where the latter formed instantaneously.

Mud Turbidites and Contourites

In the lower sediment sequence of site 124 of the JOIDES drilling, rhythmically interbedded light- and dark-colored marl oozes occur (see

[3] We have opted for the term "hemipelagic," as opposed to "pelagic," in describing the type B (e^B) muds. Pelagic sediments have been defined as "Deep-sea sediments without terrigenous material; they are either inorganic red clay or organic ooze" (AGI Glossary of Geology, 1972). Hemipelagic sediments are defined as "Deep-sea sediments containing a small amount of terrigenous material as well as remains of pelagic organisms" (AGI Glossary of Geology, 1972). Authors differ on the amount and size of terrigenous matter. Kuenen (1950) defines hemipelagic sediments as those with mainly pelagic but little terrigenous matter, while Kukal (1971) defines these as containing more than 20 percent of terrigenous material of silt and sand grade.

"Geographic and Geologic Setting"). The dark-colored oozes can start with sand-silt laminae and are more terrigenous in composition. The light-colored oozes contain predominantly particles of pelagic origin. The lower limit of the dark-colored layers can be sharp, or can be diffuse due to burrowing. These rhythmically interbedded sediments are interpreted by Ryan, Hsü, et al. (1973a) as contourites, formed by currents on the sea floor associated with a strong thermohaline circulation. The alternating fine-grained layers are quite similar to the type 3 rhythm of this study (Figure 4), in which a turbiditic mud layer, beginning with a thin coarse-grained lamina or lamel, is followed by a hemipelagic mud layer. From the description of these rhythmically interbedded fine-grained layers in the initial report of Leg XIII drilling (Ryan, Hsü, et al., 1973c) no convincing evidence appears that these deposits are contourites. The description suggests that they resemble closely an alternation of mud turbidites and pelagic deposits. However, the evidence for bottom current activity provided by coarse foram test concentrations, also reported in this sequence, is not disputed here. These foram test pavements are similar to those interpreted in this study as winnowed concentrates.

Ancient Flysch and Flysch-like Successions

The results of this study should be tested in other deep-sea basins. It is important that cores be examined by X-radiography prior to hardening, since it provides information needed to identify mud types.

The distinctive properties of the turbiditic and hemipelagic mud layers in the Algéro-Balearic Basin could prove useful in the study of flysch shales (see "Introduction"). Also, the sedimentology and paleogeography of the numerous, sometimes thick, shaly, flysch-like successions in ancient geosynclinal belts (flysch noire, Helminthoides flysch, argile scagliose, blue marl, etc.) remain largely enigmas. The combined radiographic-granulometric-compositional method used in this study could best be applied to relatively fresh, unbroken shale slabs (Hall and Stanley, 1973) or core sections. The identification of possible rhythms in these shale samples would be a first step in determining the depositional history of these flysch-like formations.

Radiocarbon Ages and Rates of Sedimentation

Ages of ten samples from five different cores (7, 9, 9A, 10, 10A) were obtained by radiocarbon determinations (Figure 6). The samples selected for C^{14} dating consisted of carbonate sand (predominantly pteropod shells and foram tests) sieved from hemipelagic layers. In addition, two samples from core 10 consisted of carbonate sand from two sand turbidite layers. Lack of sufficient concentrations of carbonate sand in other layers prevented taking more than twelve samples for dating purposes. The position and the extent of the sampled mud and sand layers are indicated in Figure 6. The ages are given in Table 8.

In Figure 21 the sample dates (ages) are plotted (1) versus the total sediment thickness (depth in cores) and (2) versus the combined thicknesses (depth in cores) of the hemipelagic layers only, leaving out the turbiditic intercalations. For both plots the correlation coefficients between age and thickness of the sediments plus the regression lines are indicated. For the total sediment thickness the values are: $r=0.93$, and $y=22.7\times51.3$. For the hemipelagic sediment thickness these are : $r=0.98$, and $y=9.7\times8.1$. Both correlations are statistically significant at the 0.05 level of confidence.

As might be expected, the correlation for the combined hemipelagic thickness only is stronger than that for total sediment (hemipelagic plus turbiditic) thicknesss; the latter includes a considerable number of instantaneously deposited

Table 8.—*Radiocarbon dates determined on the carbonate sand fraction of ten hemipelagic mud layers and two turbidite sand layers*

Core no.	*Rhythm no.*	*Carbon dating code*	*Radiocarbon date*	*Carbonate sand sieved from*
7	17	SI-1429	6215 ± 180	Hemipelagic mud
7	11	SI-1430	14,810 ± 275	Hemipelagic mud
9	12	SI-1431	2780 ± 50	Hemipelagic mud
9	7	SI-1432	11,915 ± 200	Hemipelagic mud
9	3	SI-1433	16,165 ± 310	Hemipelagic mud
9A	17	SI-1434	6135 ± 125	Hemipelagic mud
9A	10	SI-1435	12,605 ± 190	Hemipelagic mud
10	12	SI-1436	21,205 ± 330	Turbidite sand
10	5	SI-1437	29,650 ± 1180	Turbidite sand
10A	26	SI-1438	2590 ± 75	Hemipelagic mud
10A	20	SI-1439	12,460 ± 230	Hemipelagic mud
10A	2	SI-1440	> 41,000	Hemipelagic mud

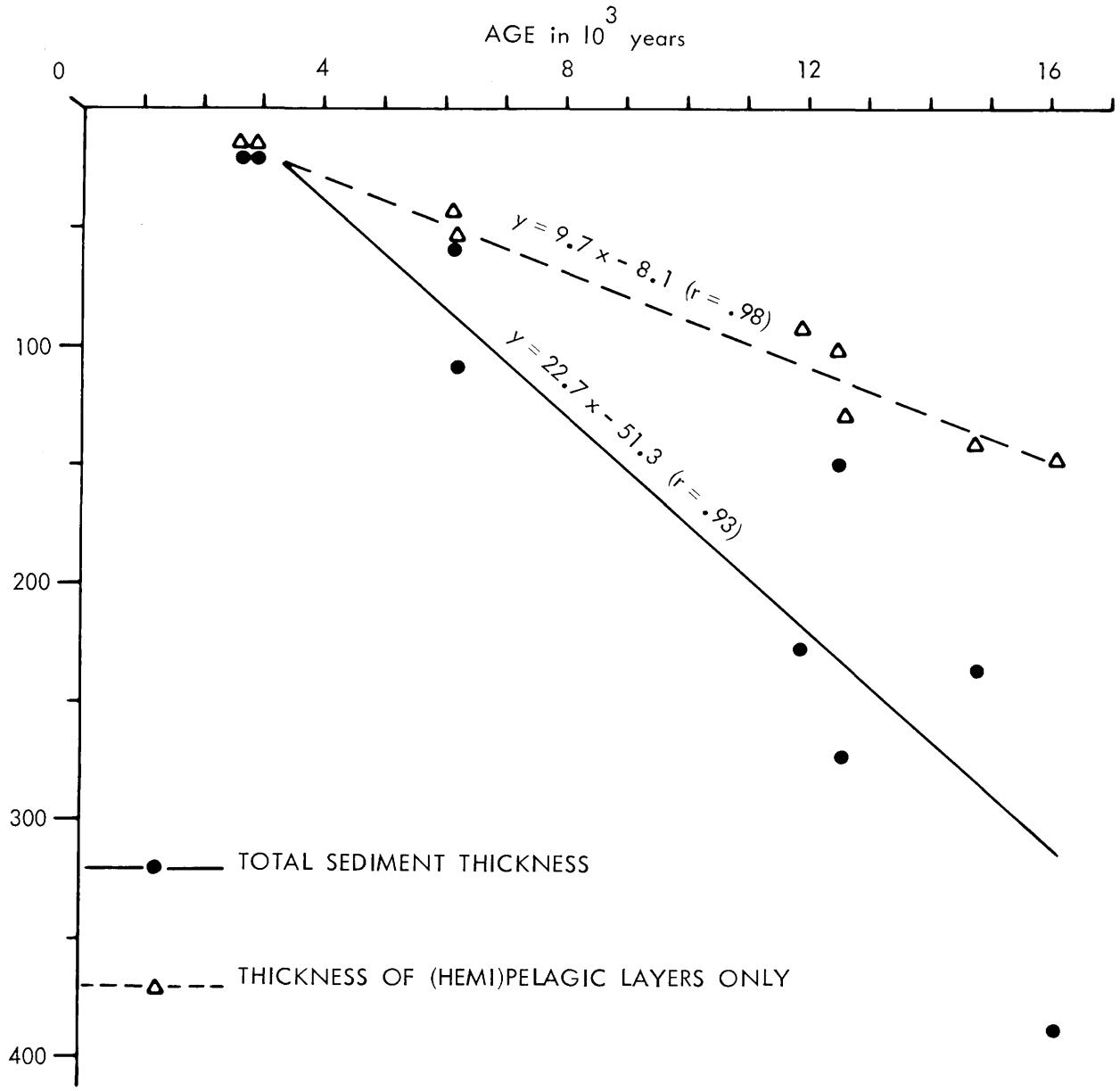

FIGURE 21.—Graph of ten radiocarbon dates from carbonate sands of hemipelagic (type B mud) layers versus (1) total depth in the core of the respective layers (solid line), and (2) the combined thicknesses of hemipelagic mud layers only, omitting the turbiditic sections (dashed line).

mud, silt, and sand-turbidite layers distributed irregularly throughout the cores examined (Figure 6). The virtually perfect correlation for the hemipelagic layers only is in accordance with a continuous pelagic settling process. The sedimentation rate for these layers is almost exactly the same in all cores throughout the Abyssal Plain. In contrast, the total sedimentation rate differs markedly from core to core.

The following sedimentation rates are inferred from the plots in Figure 21: total sediment thickness, 23 cm/1000 years (this value is only an

average for all cores combined); hemipelagic sediment thickness, 10 cm/1000 years (virtually a constant value in all cores, confirming the interpretation of their hemipelagic origin). These rates correspond to 230 Bubnoff units and 100 B respectively (Fischer 1969). The core-to-core variation in sedimentation rates is illustrated in Figure 6, where 5000-year isochrons are drawn between the cores. These isochrons have been calculated based on the sedimentation rate for the hemipelagic layers of 10 cm/1000 years.

In core 10, the ages of the turbidite carbonates are much older than those indicated by the isochrons. This fits the theory that the sampled layers include much older materials that were redeposited by turbidity currents. By interpolation between the two turbidite dates, it is possible to calculate the following sedimentation rates: for the total sediment thickness, 33 cm/1000 years (331 B), and for the pelagic layers, 10 cm/1000 years (104 B). The latter value approximates the pelagic rate as determined from the other samples (Figure 21).

The almost perfect correlation between age and depth (thickness) of the hemipelagic layers indicates that no significant erosion of these layers by bottom or turbidity currents has occurred. Little or no erosion by the turbidity currents is to be expected in a distal setting where the majority of the turbidity currents deposit mud turbidites.

The negative intercept in the regression lines in Figure 21 could imply a reduction in sedimentation rate during the past several thousand years. Another possible explanation, however, is compaction: with increasing depth, the compaction increases and the age-depth relationship changes from a straight to a curved line. In any case, it is known that total sedimentation rate in the western Mediterranean has not been constant during much of Quaternary time, due in large part to climatic and eustatic changes affecting the circum-Mediterranean region (Mars, 1963). Rates have decreased considerably since the end of the Pleistocene (Bartolini and Gehin, 1970; Leclaire, 1972a; Huang, Stanley, and Stuckenrath, 1972).

The isochrons in Figure 6 show that, except for cores 8 and 8A, all cores extend backward from the postglacial (11,000 B.P., Leclaire, 1972a) into the Late Würm. Cores 8 and 8A, lying at the greatest water depths, display the highest overall sedimentation rate. The area which they occupy probably has had a greater access to sediments derived from the important oueds (Soummam, el Kebir, etc.) on the eastern Algerian margin; turbidity currents redeposit these materials downslope, as they flow toward the deepest basin plain off western Sardinia. Turbidity currents have been triggered by earthquakes (Heezen and Ewing, 1955) and perhaps also by storms and phases of high-river discharge, as in the northern Balearic Basin (Gennesseaux, Guibout, and Lacombe, 1971). Although cores 7, 10, and 10A lie closer to the base of fans, the relatively low proportion of sand and mud turbidites suggest that they probably occupy sectors of the sea floor somewhat more shielded from sediment sources by topographic features such as levees (Figure 1).

Other studies indicate that the average sedimentation rate for the upper 300 m of section (lower Pliocene-Pleistocene) at JOIDES site 124 is 9 cm/1000 years, and that of the Quaternary section at site 133 exceeds 13 cm/1000 years (Ryan, Hsü, et al., 1973b). Rates of 12 to 100 cm/1000 years are calculated for deposits at the base of the slope off Algeria (Leclaire, 1972a). However, the sedimentation rates of our study are of the same order of magnitude as those calculated by others for the Late Pleistocene-Holocene in the western Mediterranean in its deep parts. Gennesseaux and Thommeret (1968) calculate rates of 30 cm/1000 years in the northern part of the Balearic Basin. Eriksson (1965) puts the total sedimentation rate of core 210 southeast of our core 10A at 35 cm/1000 years, and he estimates the pelagic rate at between 14 cm to 29 cm/1000 years. The latter values are higher than ours, however, inasmuch as Eriksson was unable to make a precise distinction between turbiditic and pelagic mud layers, and he included part of the former for his pelagic rate calculations. In the neighboring Alboran Sea, Vergnaud-Grazzini and Bartolini (1970) calculate rates of 26 to 30 cm/1000 years and Huang and Stanley (1972) calculate a rate of sedimentation during the past 10,000 years of 30 to 40 cm/1000 years in the basin plain and about 20 cm/1000 years on slopes. These somewhat higher rates reflect the closer proximity to the North African and Iberian Margin and greater access to sediments transported by turbidity currents and gravity-assisted flows; these studies also disregard the dis-

tinction between turbiditic and pelagic muds.

The frequency of turbidity currents has been calculated on the basis of radiocarbon ages and the isochrons computed with the aid of these. The average frequency is 3 turbidity currents per 2000 years; the turbidity current frequency differs greatly from core to core across the Algéro-Balearic Basin. From core 7 to core 10A these frequencies number as follows: 12, 30, 30, 8, 18, 9, and 12 per 12,000 years. The average frequency of 3 turbidity currents per 2000 years applies to the seven localities examined within the Abyssal Plain. It should be pointed out that single turbidites were not correlated between cores, and it is unlikely that their individual beds extend over most of the basin floor covered by the cores. Thus, the 3 turbidites per 2000 years reflect different turbidity currents at widely separated core localities. In other words, the basin plain as a whole received considerably more than 3 incursions per 2000 years.

In other basins, such as the middle of the San Pedro and Santa Monica basins off California, the frequency of turbidity currents is estimated at 1 every 400 years (Gorsline and Emery, 1959). Most other frequency estimates are significantly lower. In the Bahamas region, for instance, the frequency varies from 1 per 500 years to 1 per 10,000 years in the Tongue of the Ocean (Rusnak and Nesteroff, 1964), and 1 per 3000 to 6000 years in the Columbus Basin (Bornhold and Pilkey, 1971). Estimates for ancient flysch occurrences are 1 turbidite per 2000 years (Moore, 1971), or per 4000 years (Sujkowski, 1957). The much higher average turbidity current frequency in the Algéro-Balearic Basin (more than 3 incursions per 2000 years) is in part based on the fact that mud turbidites can be recognized in this study.

Conclusions

1. Sediment cores from the Algéro-Balearic Abyssal Plain, western Mediterranean, contain large sections of mud, seemingly homogeneous. Use of X-radiographs of split cores enables the distinction between two different types of mud, and the recognition of a large number of mud layers, alternating in a regular fashion.

2. The color of the sediment is not a reliable criterion to distinguish between different mud layers and to determine their boundaries.

3. Structural, textural, and compositional properties of the two mud types indicate that one type is deposited by turbidity currents, and the other by pelagic settling. Incidental reworking of hemipelagic muds by bottom currents has occurred.

4. Among the many properties of the turbiditic muds, the most characteristic are: structural, textural, and compositional continuity between underlying sand-silt turbidites and the muds, grading within the mud layers, and a very small amount of sand-size material ($\leq$ 1 percent).

5. The most distinctive properties of the hemipelagic muds are: they are entirely unlaminated, display exclusively burrow structures, a sizable amount of sand-size material is present (an average of 8 percent), the coarse components are dominantly made up of pelagic foram tests and pteropod shells, their grain-size distribution is nearly normal with a median around 9 phi, they are very poorly sorted, and in general their properties are virtually uniform between muds from different sediment depths and core locations.

6. The boundary between the two mud types is most distinctly marked by changes in the amount of sand-grade material, the proportion of remains of pteropods and pelagic forams, and the proportion of mica.

7. When the mud turbidite is markedly terrigenous in composition, the ratios of illite, chlorite, and kaolinite differ between a turbiditic mud and the overlying hemipelagic mud. This observation is of consequence to studies of paleoclimatological change based on clay mineralogy.

8. The distinction between turbiditic and hemipelagic muds in the cores enables an accurate estimate of pelagic sedimentation rate from radiocarbon dates on pelagic carbonate sands. During the past 16,000 years this rate has been 10 cm/1000 years.

9. This distinction coupled with the radiocarbon dates also makes possible an accurate estimate of the frequency of turbidity current incursions in the Balearic Basin. The average frequency for the past 20,000 years or so has been 3 incursions per 2000 years in a particular core locality. The number for the basin as a whole should be higher.

10. The seven analyzed cores from across the southern Balearic Abyssal Plain show a facies of alternating sand-silt and silt turbidites, mud turbidites (locally more than half of the core section),

and hemipelagic muds (more than half in some cores). The two mud types have as yet not been distinguished to this degree in ancient deep marine successions. Largely shaly or marly flysch facies are known, and these may bear some analogies with the muddy turbiditic-hemipelagic sequences of the southern Balearic Abyssal Plain examined in this study. Comparison of similar ancient and modern deepwater, mud-rich deposits warrants further analysis.

Literature Cited

Auzende, J. M., J. Bonnin, and J. L. Olivet
1973. The Origin of the Western Mediterranean Basin. *Journal of the Geological Society of London,* 129: 607–620.

Barazangi, M., and J. Dorman
1969. World Seismicity Maps Compiled from ESSA Coast and Geodetic Survey Epicenter Data 1961–1967. *Bulletin of the Seismological Society of America,* 59:369–380.

Bartolini, C., and C. E. Gehin
1970. Evidence of Sedimentation by Gravity-assisted Bottom Currents in the Mediterranean Sea. *Marine Geology,* 9:M1–M5.

Bellaiche, G., H. Chamley, and F. Rotschy
1972. Quelques particularitiés de la sédimentation marine quaternaire au sud de l'Ile du Levant (Var). *Tethys,* 4 (1):243–250.

Bornhold, B. D., and O. H. Pilkey
1971. Bioclastic Turbidite Sedimentation in Columbus Basin, Bahamas. *Bulletin of the Geological Society of America,* 82:1341–1354.

Bouma, A. H.
1962. *Sedimentology of Some Flysch Deposits: A Graphic Approach to Facies Interpretation.* 168 pages. Amsterdam: Elsevier.
1972a. Recent and Ancient Turbidites and Contourites. *Transactions of the Gulf Coast Association of Geological Societies,* 22:205–221.
1972b. Fossil Contourites in Lower Niesenflysch, Switzerland. *Journal of Sedimentary Petrology,* 42 (4):917–921.

Bourcart, J.
1959. Morphologie du précontinent des Pyrenées à la Sardaigne. Pages 33–52 in *La topographie et la géologie des profondeurs océaniques, colloques internationaux C.N.R.S., Nice-Villefranche.*

Carter, T. G., J. P. Flanagan, et al.
1972. A New Bathymetric Chart and Physiography of the Mediterranean Sea. Pages 1–24 *in* D. J. Stanley, editor, *The Mediterranean Sea: A Natural Sedimentation Laboratory.* Stroudsburg: Dowden, Hutchinson and Ross, Inc.

Cline, L. M.
1970. Sedimentary Features of Late Paleozoic Flysch, Ouachita Mountains, Oklahoma. *The Geological Association of Canada, Special Paper,* 7:85–101.

Comas, M. C.
1968. Existencia de un flysch nummulitico en el sector de Moreda (Zona Subbetica) Provincia de Granada. *Boletin del Instituto de Estudios Asturianos,* number 14.

Davies, D. K.
1968. Carbonate Turbidites, Gulf of Mexico. *Journal of Sedimentary Petrology,* 38 (4):1100–1109.

Dewey, J. F., W. C. Pitman III, W. B. F. Ryan, and J. Bonin
1973. Plate Tectonics and the Evolution of the Alpine System. *Bulletin of the Geological Society of America,* 84:3137–3180.

Dzulynski, S., M. Ksiazkiewicz, and Ph. H. Kuenen
1959. Turbidites in Flysch of the Polish Carpathian Mountains. *Bulletin of the Geological Society of America,* 70:1089–1118.

Dzulynski, S., and A. J. Smith
1964. Flysch Facies. *Annales de la Société Géologique de Pologne,* 34:245–266.

Enos, P.
1969. Anatomy of a Flysch. *Journal of Sedimentary Petrology,* 39 (2):680–723.

Ericson, D. B., M. Ewing, and B. C. Heezen
1952. Turbidity Currents and Sediments in North America. *Bulletin of the American Association of Petroleum Geologists,* 36:489–511.

Eriksson, K. G.
1965. The Sediment Core No. 210 from the Western Mediterranean Sea. In *Reports of the Swedish Deep-Sea Expedition, 1947–48,* 8:397–594.

Ewing, M., and E. M. Thorndike
1965. Suspended Matter in Deep Ocean Water. *Science,* 147:1291–1294.

Fischer, A. G.
1969. Geological Time-Distance Rates: The Bubnoff Unit. *Bulletin of the Geological Society of America,* 80: 549–552.

Fleischer, P.
1972. Mineralogy and Sedimentation History, Santa Barbara Basin, California. *Journal of Sedimentary Petrology,* 42 (1):49–58.

Folk, R. L.
1961. *Petrology of Sedimentary Rocks.* 154 pages. The University of Texas.

Folk, R. L., and W. C. Ward
1957. Brazos River Bar, a Study in the Significance of Grain-size Parameters. *Journal of Sedimentary Petrology,* 27:3–27.

Gennesseaux, M., and Y. Thommeret
1968. Datation par le radiocarbone de quelques sédiments

sous-marins de la Région Niçoise. *Revue de Géographie Physique et de Géologie Dynamique,* 10: 375–382.

Gennesseaux, M., P. Guibout, and H. Lacombe
1971. Enrégistrement de courants de turbidité dans la vallée sous-marine du Var (Alpes-Maritimes). *Comptes Rendus de l'Académie des Sciences de Paris,* 273:2456–2459.

Gorsline, D. S., and K. O. Emery
1959. Turbidity-current Deposits in San Pedro and Santa Monica Basins off Southern California. *Bulletin of the Geological Society of America,* 70:279–290.

Hall, B. A., and D. J. Stanley
1973. Levee-bounded Submarine Base-of-Slope Channels in the Lower Devonian Seboomook Formation, Northern Maine. *Bulletin of the Geological Society of America,* 84:2101–2110.

Heezen, B. C., and M. Ewing
1955. Orleansville Earthquake and Turbidity Currents. *Bulletin of the American Association of Petroleum Geologists,* 39:2505–2514.

Heezen, B. C., and C. D. Hollister
1971. *The Face of the Deep.* 659 pages. New York: Oxford University Press.

Heezen, B. C., C. D. Hollister, and W. T. Ruddiman
1966. Shaping of the Continental Rise by Deep Geostrophic Contour Currents. *Science,* 152:502–508.

Hesse, R., and U. von Rad
1972. Undisturbed Large-Diameter Cores from the Strait of Otranto. Pages 645–654 *in* D. J. Stanley, editor, *The Mediterranean Sea: A Natural Sedimentation Laboratory.* Stroudsburg: Dowden, Hutchinson, and Ross, Inc.

Holtedahl, H.
1965. Recent Turbidites in the Hardangerfjord, Norway. Pages 107–141 *in* W. F. Whittard, and R. Bradshaw, editors, *Submarine Geology and Geophysics.* London: Butterworths.

Horn, D. R., J. I. Ewing, and M. Ewing
1972. Graded-Bed Sequences Emplaced by Turbidity Currents North of 20°N in the Pacific, Atlantic and Mediterranean. *Sedimentology,* 12:283–275.

Hsü, K. J.
1971. Origin of the Alps and Western Mediterranean. *Nature,* 233 (5314):44–48.

Huang, T.-C., and J. W. Pierce
1971. The Carbonate Minerals of Deep-Sea Bioclastic Turbidites, Southern Blake Basin. *Journal of Sedimentary Petrology,* 41 (1):251–260.

Huang, T.-C., and D. J. Stanley
1972. Western Alboran Sea: Sediment Dispersal, Ponding and Reversal of Currents. Pages 521–559 *in* D. J. Stanley, editor, *The Mediterranean Sea: A Natural Sedimentation Laboratory.* Stroudsburg: Dowden, Hutchinson, and Ross, Inc.

Huang, T.-C., D. J. Stanley, and R. Stuckenrath
1972. Sedimentological Evidence for Current Reversal at the Strait of Gibraltar. *Marine Technology Journal,* 6 (4):25–33.

Hubert, J. F.
1964. Textural Evidence for Deposition of Many Western North Atlantic Deep-Sea Sands by Ocean-Bottom Currents Rather than Turbidity Currents. *Journal of Geology,* 72:757–785.

Kelling, G., and D. J. Stanley
1972a. Sedimentary Evidence of Bottom Current Activity, Strait of Gibraltar Region. *Marine Geology,* 13: M51–M60.
1972b. Sedimentation in the Vicinity of the Strait of Gilbraltar. Pages 489–520 *in* D. J. Stanley, editor, *The Mediterranean Sea: A Natural Sedimentation Laboratory.* Stroudsburg: Dowden, Hutchinson, and Ross, Inc.

Ksiazkiewicz, M.
1961. Life Conditions in Flysch Basins. *Annales de la Société Géologique de Pologne,* 31 (1):3–21.

Kuenen, Ph. H.
1950. *Marine Geology.* 568 pages. New York: John Wiley and Sons.
1964. The Shell Pavement below Oceanic Turbidites. *Marine Geology,* 2:236–246.
1967. Emplacement of Flysch-Type Sand Beds. *Sedimentology,* 9:203–243.

Kukal, Z.
1971. *Geology of Recent Sediments.* 490 pages. London and New York: Academic Press.

Lacombe, H.
1971. Le détroit de Gilbraltar; Océanographie physique. *Mémoires du Service Géologique du Maroc,* 222 bis.

Lacombe, H., and P. Tchernia
1972. Caractères hydrologiques et circulation des eaux en Méditerranée. Pages 25–36 *in* D. J. Stanley, editor, *The Mediterranean Sea: A Natural Sedimentation Laboratory.* Stroudsburg: Dowden, Hutchinson, and Ross, Inc.

Leclaire, L.
1972a. Aspects of Late Quaternary Sedimentation on the Algerian Precontinent and in the Adjacent Algiers-Balearic Basin. Pages 561–582 *in* D. J. Stanley, editor, *The Mediterranean Sea: A Natural Sedimentation Laboratory.* Stroudsburg: Dowden, Hutchinson, and Ross, Inc.
1972b. La sédimentation holocène sur le versant Méridional du Bassin Algéro-Baléare (Précontinent Algérien). *Mémoires du Muséum National d'Histoire Naturelle,* 24: 291 pages.

Mars, P.
1963. Les faunes et la stratigraphie du quaternaire Méditerranéen. *Recueil des Traveaux Station Maritime d'Endoume,* 28:61–97.

McBride, E. F.
1970. Flysch Sedimentation in the Marathon Region, Texas. *The Geological Association of Canada, Special Paper,* 7:67–83.

McKenzie, D. P.
1970. Plate Tectonics of the Mediterranean Region. *Nature,* 226:239–243.

Menard, H. W., S. M. Smith, and R. M. Pratt
1965. The Rhone Deep-Sea Fan. Pages 271–285 *in* W. F. Whittard and R. Bradshaw, editors, *Submarine Geology and Geophysics.* London: Butterworth.

Middleton, G. V., editor
1965. Primary Sedimentary Structures and Their Hydrodynamic Interpretation. *Society of Economic Paleontologists and Mineralogists, Special Publication Number* 12: 265 pages.
1967. Experiments on Density and Turbidity Currents, III: Deposition of Sediment. *Canadian Journal of Earth Science,* 4:475–505.

Miller, A. R.
1972. Speculations Concerning Bottom Circulation in the Mediterranean Sea. Pages 37–42 *in* D. J. Stanley, editor, *The Mediterranean Sea: A Natural Sedimentation Laboratory.* Stroudsburg: Dowden, Hutchinson, and Ross, Inc.

Moore, B. R.
1971. Paleographic and Tectonic Significance of Diachronism in Siluro-Devonian Age Flysch Sediments, Melbourne Trough, Southeastern Australia. *Bulletin of the Geological Society of America,* 82:1087–1094.

Moore, D. G.
1969. Reflection Profiling Studies of the California Continental Borderland: Structure and Quaternary Turbidite Basins. *Geological Society of America Special Paper,* 107: 142 pages.

Moores, H. T.
1969. The Position of Graptolites in Turbidites. *Sedimentary Geology,* 3:241–261.

Natland, M. L.
1963. Paleoecology and Turbidites. *Journal of Paleontology,* 37:946–951.

Nederlof, M. H.
1959. Structure and Sedimentology of the Upper Carboniferous of the Upper Pisuerga Valleys, Cantabrian Mountains, Spain. *Leidse Geologische Mededelingen,* 24:603–703.

Nesteroff, W. D.
1961. La "Séquence Type" dans les turbidites terrigènes Modernes. *Revue de Géographie Physique et de Géologie Dynamique,* 4 (2):263–268.
1973. Distribution of the Fine-Grained Sediment Component in the Mediterranean. Pages 666–670 *in* Volume XIII *in* W. B. F. Ryan, K. J. Hsü, et al., editors, *Initial Reports of the Deep Sea Drilling Project.* Washington: U.S. Government Printing Office.

Nesteroff, W. D., and B. C. Heezen
1963. Essais de comparaison entre les turbidites modernes et le Flysch. *Revue de Géographie Physique et Géologie Dynamique,* 5 (2):115–127.

Nesteroff, W. D., W. B. F. Ryan, et al.
1972. Evolution de la sédimentation pendant le néogène en Méditerranée d'après les forages JOIDES-DSDP. Pages 47–62 *in* D. J. Stanley, editor, *The Mediterranean Sea: A Natural Sedimentation Laboratory.* Stroudsburg: Dowden, Hutchinson, and Ross, Inc.

Nesteroff, W. D., G. Sabatier, and B. C. Heezen
1965. Les minéraux argileux dans les sédiments du bassin occidental de la Méditerranée. *Commission Internationale pour l'Etude Scientifique de la Mer Méditerranée,* 17 (3):1005–1007.

Nesteroff, W. D., F. C. Wezel, and G. Pautot
1973. Summary of Lithostratigraphic Findings and Problems. Pages 1021–1040 *in* Volume XIII *in* W. B. F. Ryan, K. J. Hsü, et al., editors, *Initial Reports of the Deep Sea Drilling Project.* Washington: U.S. Government Printing Office.

Olausson, E.
1960. Description of Sediment Cores from the Mediterranean and the Red Sea. *Reports of the Swedish Deep-Sea Expedition,* 8 (5):327–334.

Pannekoek, A. J.
1969. Uplift and Subsidence in and around the Western Mediterranean since the Oligocene: A Review. *Verhandelingen van het Koninklijk Nederlands Geologisch en Mijnbouwkundig Genootschap,* 26:53–77.

Parker, F. L.
1958. Eastern Mediterranean Foraminifera. *Reports of the Swedish Deep-Sea Expedition,* 8 (4):219–283.

Piper, D. J. W.
1972. Turbidite Origin of Some Laminated Mudstones. *Geological Magazine,* 109 (2):115–126.
1973. The Sedimentology of Silt Turbidites from the Gulf of Alaska. Pages 847–867 *in* Volume XVII *in* L. D. Kulm, R. von Huene, et al., editors, *Initial Reports of the Deep Sea Drilling Project.* Washington, D.C.: U.S. Government Printing Office.

Radomski, A.
1958. The Sedimentological Character of the Podhale Flysch. *Acta Geologica Pologna,* 8:335–410.
1960. Remarks on Sedimentation of Shales in Flysch Deposits. *Bulletin de l'Académie des Sciences de Pologne, Série des Sciences Géologique et Géographique,* 8 (2):123–129.

Ritsema, A. R.
1969. Seismic Data of the Western Mediterranean and the Problem of Occanization. *Verhandelingen van het Koninklijk Nederlands Geologisch Mijnbouwkundig Genootschap,* 26:105–120.

Rupke, N. A.
1969. Aspects of Bed Thickness in Some Eocene Turbidite Sequences. *Journal of Geology,* 77:482–484.
1972. *Geologic Studies of an Early and Middle Eocene Flysch Formation, Southwestern Pyrenees, Spain.* Doctoral disseration, Princeton University.

Rusnak, G. A., and W. D. Nesteroff
1964. Modern Turbidites: Terrigenous Abyssal Plain versus Bioclastic Basin. Pages 448–507 *in* R. L.

Miller, editor, *Papers in Marine Geology, Shepard Commemorative Volume*. New York: Macmillan Co.

Ryan, W. B. F., and K. J. Hsü, et al.
1973a. Balearic Rise – Site 124. Pages 133–174 *in* Volume XIII *in* W. B. F. Ryan, K. J. Hsü, et al. editors, *Initial Reports of the Deep Sea Drilling Project*. Washington, D.C.: U.S. Government Printing Office.
1973b. Boundery of Sardinia Slope with Balearic Abyssal Plain – Sites 133 and 134. Pages 465–514 *in* Volume XIII *in* W. B. F. Ryan, K. J. Hsü, et al., editors, *Initial Reports of the Deep Sea Drilling Project*. Washington, D.C.: U.S. Government Printing Office.

Ryan, W. B. F., and K. J. Hsü, et al., editors
1973c. Volume XIII. In *Initial Reports of the Deep Sea Drilling Project*. 1447 pages. Washington, D.C.: U.S. Government Printing Office.

Ryan, W. B. F., D. J. Stanley, J. B. Hersey, D. A. Fahlquist, and T. D. Allan
1969. The Tectonics and Geology of the Mediterranean Sea. Pages 389–492 *in* Volume 4 *in* J. C. Maxwell, editor, *The Sea*. New York: John Wiley and Sons.

Semple, E. C.
1931. *The Geography of the Mediterranean Region*. 737 pages. New York: AMS Press.

Stanley, D. J.
1963. Vertical Petrographic Variability in Annot Sandstone Turbidites: Some Preliminary Observations and Generalizations. *Journal of Sedimentary Petrology*, 33:783–788.
1970. Flyschoid Sedimentation on the Outer Atlantic Margin off Northeast North America. *The Geological Association of Canada, Special Paper*, 7:179–210.

Stanley, D. J., editor
1969. *The New Concepts of Continental Margin Sedimentation*. 400 pages. Washington D.C.: American Geological Institute.

Stanley, D. J., and L. Diester-Haass
1973. Modern Basin Sediment Deformation by Salt Tectonics, Western Mediterranean. *Abstracts of the European Geophysical Society, Zürich*, page 97.

Stanley, D. J., C. E. Gehin, and C. Bartolini
1970. Flysch-type Sedimentation in the Alboran Sea, Western Mediterranean. *Nature*, 228:979–983.

Stanley, D. J., H. Sheng, and C. P. Pedraza
1971. Lower Continental Rise East of the Middle Atlantic States: Predominant Sediment Dispersal Perpendicular to Isobaths. *Bulletin of the Geological Society of America*, 82:1831–1840.

Stommel, H., A. Voorhis, and D. Webb
1971. Submarine Clouds in the Deep Ocean. *American Scientist*, 59:716–722.

Sujkowski, Zb. L.
1957. Flysch Sedimentation. *Bulletin of the Geological Society of America*, 68:543–554.

Tanaka, K.
1970. Sedimentation of the Cretaceous Flysch Sequence in the Ikushumbetsu Area, Hokkaido, Japan. *Geological Survey of Japan Report*, 236: 102 pages.

Van Andel, Tj. H., and P. D. Komar
1969. Ponded Sediments of the Mid-Atlantic Ridge Between 22° and 23° North Latitude. *Bulletin of the Geological Society of America*, 80:1163–1190.

Van Bemmelen, R. W.
1969. Origin of the Western Mediterranean Sea. *Verhandelingen van het Koninklijk Nederlands Geologisch en Mijnbouwkundig Genootschap*, 26:13–52.

Van Hinte, J. E.
1963. Zur Stratigraphie und Mikropaläontologie der Oberkreide und des Eozans des Krappfeldes (Kärnten). *Jahrbuch der Geologischen Bundesanstalt, Wien*, 8: 147 pages.

Van Straaten, L. M. J. U.
1966. Micro-Malacological Investigation of Cores from the Southeastern Adriatic Sea. *Koninklijke Nederlandse Akademie van Wetenschappen, Amsterdam, Verhandelingen*, series B, 69:429–445.
1967. Turbidites, Ash Layers and Shell Beds in the Bathyal Zone of the Southeastern Adriatic Sea. *Revue de Géographie Physique et de Géologie Dynamique*, 9 (3):219–240.
1970. Holocene and Late-Pleistocene Sedimentation in the Adriatic Sea. *Geologische Rundschau*, 60:106–131.

Vergnaud-Grazzini, C., and C. Bartolini
1970. Evolution Paléoclimatique des Sédiments Würmiens et Post-Würmiens en mer d'Alboran. *Revue de Géographie Physique et de Géologie Dynamique*, 12:325–334.

Vita-Finzi, C.
1972. Supply of Fluvial Sediment to the Mediterranean during the Last 20,000 Years. Pages 43–46 *in* D. J. Stanley, editor, *The Mediterranean Sea: A Natural Sedimentation Laboratory*. Stroudsburg: Dowden, Hutchinson, and Ross, Inc.

Vogt, P. R., R. H. Higgs, and G. L. Johnson
1971. Hypotheses on the Origin of the Mediterranean Basin: Magnetic Data. *Journal of Geophysical Research*, 76 (14):3207–3228.

Walker, R. G.
1967. Turbidite Sedimentary Structures and Their Relationship to Proximal and Distal Depositional Environments. *Journal of Sedimentary Petrology*, 37: 25–43.
1970. Review of the Geometry and Facies Organization of Turbidites and Turbidite-Bearing Basins. *The Geological Association of Canada, Special Paper*, 7:219–251.

Watson, J. A., and G. L. Johnson
1969. The Marine Geophysical Survey in the Mediterranean. *International Hydrographic Review*, 46: 81–107.

Weidmann, M.
1967. Petite contribution à la connaissance du Flysch. *Bulletin des Laboratoires de Géologie, Minéralogie, Géophysique et du Musée Géologique de l'Université de Lausanne*, 166: 6 pages.

Weiler, Y.
1969. The Miocene Kythrea Flysch Basin in Cyprus. In Committee Mediterranean Neogene Stratigraphy, Proceedings of the IV Session, Bologna, 1967. *Giornale di Geologia* (2), 35 (4):213–229.

Wezel, F. C., and W. B. F. Ryan
1971. Flysch, margini continentali e zolle litosferiche. *Bollettino della Societa di Geologia,* 90: 249 pages.

Wüst, G.
1960. Die Tiefenzirkulation des Mittellandischen Meeres in den Kernschichten des Zwischen–und des Tiefenwassers. *Deutsche Hydrographische Zeitschrift,* 13:105–131.

☆ U.S. GOVERNMENT PRINTING OFFICE: 1974—546–363/19